

# Spiral Galaxies with HST/NICMOS. I. Nuclear Morphologies, Color Maps and Distinct Nuclei<sup>1</sup>

C. Marcella Carollo<sup>2</sup>

Columbia University, Department of Astronomy, 538 W. 120<sup>th</sup> St., New York, NY 10027

Massimo Stiavelli

Space Telescope Science Institute, 3700 San Martin Drive, Baltimore MD 21218

Marc Seigar<sup>3</sup>

Sterrenkundig Observatorium, Universiteit Gent, Krijgslaan 281, B-9000 Gent, Belgium

Space Telescope Science Institute, 3700 San Martin Drive, Baltimore MD 21218

P. Tim de Zeeuw

Sterrewacht Leiden, Postbus 9513, 2300 RA Leiden, The Netherlands

Herwig Dejonghe

Sterrenkundig Observatorium, Universiteit Gent, Krijgslaan 281, B-9000 Gent, Belgium

Received \_\_\_\_\_; accepted \_\_\_\_\_

---

<sup>1</sup>Based on observations with the NASA/ESA Hubble Space Telescope, obtained at the Space Telescope Science Institute, which is operated by Association of Universities for Research in Astronomy, Inc. (AURA), under NASA contract NAS5-26555

<sup>2</sup>Visiting Astronomer, The Johns Hopkins University, Department of Physics and Astronomy, Baltimore MD 21210

<sup>3</sup>Joint Astronomy Centre, 660 N. A'ohoku Place, Hilo, HI 96720

## ABSTRACT

This is the first of two papers where we present the analysis of an HST NICMOS–Cam2 near-infrared (NIR) snapshot survey in the F160W ( $H$ ) filter for a sample of 78 spiral galaxies selected from the UGC and ESOLV catalogs. For 69 of these objects we provide nuclear color information derived by combining the  $H$  data either with additional NICMOS F110W ( $J$ ) images or with  $V$  WFPC2/HST data.

Here we present the NIR images and the optical-NIR color maps. We focus our attention on the properties of the photometrically-distinct ‘nuclei’ which are found embedded in most of the galaxies, and provide measurements of their half-light radii and magnitudes in the  $H$  (and when available, in the  $J$ ) band. We find that: *(i)* In the NIR, the nuclei embedded in the bright early- to intermediate-type galaxies span a much larger range in brightness than the nuclei which are typically found embedded in bulgeless late-type disks: the nuclei embedded in the early- to intermediate-type galaxies reach on the bright end values up to  $H_{AB} \sim -17.7$  mags; *(ii)* Nuclei are found in both non-barred and barred hosts, in large-scale ( $\gtrsim 1$  kpc) as well as in nuclear (up to a few 100pc) bars; *(iii)* There is a significant increase in half-light radius with increasing luminosity of the nucleus in the early/intermediate types (a decade in radius for  $\approx 8$  magnitudes brightening), a correlation which was found in the  $V$  band and which is also seen in the NIR data; *(iv)* The nuclei of early/intermediate-type spirals cover a large range of optical-NIR colors, from  $V - H \approx -0.5$  to 3. Some nuclei are bluer and others redder than the surrounding galaxy, indicating the presence of activity or reddening by dust in many of these systems; *(v)* Some early/intermediate nuclei are elongated and/or slightly offset from the isophotal center of the host galaxy. On average, however, these nuclei appear as centered, star-cluster-like structures similar to those which are found in the late-type disks.

*subject headings:* galaxies: formation - galaxies: evolution - galaxies: structure - galaxies: nuclei - galaxies: spirals - galaxies: bulges

## 1. Introduction

The nuclear regions of spiral galaxies may hold important information concerning the growth of bulge-like structures within the disks, and more generally the secular evolution of the disks themselves. Little was known about the  $\sim 10\text{-}100$  pc scale regions of spiral galaxies before we started our HST program, a cycle 6 WFPC2 F606W ( $V$ ) survey of 75 mostly early- and intermediate-type disk galaxies selected randomly from a complete sample of 134 galaxies (Carollo et al. 1997; Carollo, Stiavelli & Mack 1998; Carollo & Stiavelli 1998; Carollo 1999). The random selection is due to the snapshot nature of the program. The unprecedented angular resolution of the HST optical images allowed probing the bulges down to absolute  $V$  magnitudes  $M_V \sim -14$ , with half-light radii  $R_e$  as small as  $\sim 100\text{pc}$ , and unveiled an astonishing richness of structure in the nuclear regions of  $\approx 60\%$  of the sample: bars, spiral-like dust lanes, star-forming rings or spiral arms. Even more surprisingly, a similar fraction of objects contains photometrically-distinct nuclear compact sources (hereafter ‘nuclei’). While a few of these nuclei appear point-like in the WFPC2 images, many are resolved with  $R_e \approx 0.1'' - 0.2''$ , corresponding to linear scales of up to  $\approx 20$  pc. The nuclei were identified primarily by visual inspection of the images, since they appear as regular, smooth structures significantly brighter than their surroundings. For the subsample of objects with a light distribution smooth enough to allow the derivation of an isophotal fit, the morphological identification of the nuclei was confirmed by inspecting the surface brightness profiles. The nuclei embedded in those hosts whose dusty/star-forming morphology did not allow us to obtain a meaningful isophotal fit are typically much brighter than the nuclei embedded in the smoother hosts, so that their identification as photometrically-distinct systems remains unambiguous. Carollo et al. (1997,1998) presented a collection of  $V$ -band images and light profiles which clearly showed the photometric decoupling between the nuclei and their underlying host galaxies. Faint nuclei embedded in bright hosts with steep nuclear stellar cusps would remain undetected (this is discussed quantitatively in the references above).

The relation between the nuclei and their galactic surroundings is unclear. In principle, the nuclei could be triggers for —and/or left-overs of— the mechanisms which produce central

structure within the disks, and could thus provide additional constraints for identifying such mechanisms. Interestingly, the WFPC2 survey has shown that many of the nuclei at the faint-end of their luminosity distribution ( $-9 \gtrsim M_V \gtrsim -12$ ) are often hosted by pseudo-bulges with an exponential —rather than  $R^{1/4}$ -law— fall-off of the light distribution (hereafter exponential bulges; Courteau, de Jong & Broeils 1996 and references therein; see also the review by Wyse, Gilmore & Franx 1997). In fact, every exponential bulge in our WFPC2 sample hosts a distinct nucleus in its center or slightly offset from it. Distinct central structures significantly different from the massive,  $R^{1/4}$ -law elliptical-like spheroids are rather common in the intermediate-type Sb-Sc disks. In the latter, in addition to the exponential bulges, pseudo-bulges have been found with cold kinematics (Kormendy 1993) or a peanut-shape morphology (Kuijken & Merrifield 1995; Bureau & Freeman 1999). The presence of the nuclei in the centers of the exponential bulges does not necessarily imply a causal connection between nuclei and bulges. At least at the heuristic level, however, such a connection may be indirectly supported on a theoretical basis, since evolutionary scenarios for bulge formation advocate for example the dissolution of a progenitor bar by means of the accumulation of a  $\sim 1\%$  central mass (Pfenniger & Norman 1990; Hasan, Pfenniger & Norman 1993; Pfenniger 1993; Norman, Sellwood & Hasan 1996, and references therein).

A first step toward understanding the nucleus-host relationship is to establish the properties of the nuclei as a function of the Hubble type and other physical properties of their parent galaxies. The findings based on the optical WFPC2 data could potentially be severely affected by large amounts of dust and of recent star formation that may be present in the central regions of spirals. To secure results less influenced by these sources of ‘pollution’, we have followed up the WFPC2 survey with a NICMOS Camera-2 F160W ( $H$ ; in some cases, also F110W, i.e., “broad”  $J$ ) snap-shot survey for the same sample of galaxies.

The analysis of our NICMOS survey is reported in this and in a companion paper (Seigar et al. 2001, paper II). In this paper we: *(i)* Introduce the NICMOS sample and describe our technique of data reduction; *(ii)* Describe the NIR images and the optical-NIR color maps of spirals at HST resolution; *(iii)* Detail the methodology used to measure the sizes and luminosities of the nuclei

from the NICMOS images, and describe the tests performed to assess the systematic errors on these measurements; *(iv)* Discuss the statistical NIR and optical-NIR properties of the nuclear regions of spirals, including the distinct nuclei, as a function of Hubble type. In paper II we present the isophotal fits to the galaxy nuclear surface brightness distribution, and the analytical fits to these profiles. Paper II also reports the derived nuclear stellar cusp slopes and the optical/NIR color profiles (for those galaxies for which both WFPC2 and NICMOS images are available). The data and measurements presented here and in paper II are used in an additional paper (Carollo et al. 2001) to discuss in more detail the nucleus-bulge connection. There we present the optical/NIR color-distribution, color-magnitude and color-color diagrams for the  $R^{1/4}$  and exponential bulges and for their nuclei, and discuss the possible implications for the formation and evolution of the central regions of early/intermediate-type disk galaxies.

In §2 we describe the NICMOS sample, the observations, the data reduction procedure and the approach adopted to derive the radii and luminosities of the nuclei. In the same section we present the tests that we performed to assess the accuracy of the measurements for the nuclei, and show the optical-NIR or NIR-NIR color maps for the target galaxies. We discuss in §3 the sizes and magnitudes of the nuclei in the NIR, their colors, as well as the structure and color of their surrounding environments. We summarize in Section 4. Consistent with our earlier work, we adopt  $H_0 = 65$  km/s/Mpc throughout this paper.

## 2. Sample and Data Analysis

The NICMOS sample presented here constitutes a random selection from the sample of 134 galaxies discussed in Carollo et al. (1997, 1998). The objects were extracted from the UGC catalog for the northern hemisphere (Nilson 1973) and the ESOLV catalog for the southern hemisphere (Lauberts & Valentijn 1989) for having angular diameter larger than 1 arcmin, redshift  $< 2500$  km s<sup>-1</sup>, inclination angle smaller than 75 degrees, and (non-barred) morphological type from Sa to Sbc. A few objects that did not satisfy these selection criteria (e.g., NGC 1365 and NGC 4565) were

however included in the final sample in substitution of objects which we were not allowed to observe due to the HST rules on duplication of targets. A posteriori, the WFPC2 images showed that the RC3 catalog (de Vaucouleurs et al. 1991) gives generally a better description of the galaxy types. Therefore, consistent with our previous WFPC2 work, we adopt in this analysis the RC3 Hubble types (with the numerical conversion given in Table 2 of RC3: 0=S0a, 1=Sa, 2=Sab, ..., 9=Sm).

## 2.1. The Dataset and the Basic Data Reduction

All NICMOS observations were performed with fine-lock guiding. 78 of the 134 systems were observed in snap-shot mode with NICMOS Camera-2 in F160W during the period June 1997 to February 1998.

Nine objects, NGC1365, NGC2903, NGC3031, NGC4536, NGC4565, NGC4569, NGC6217, NGC7479 and NGC7742 were observed with WFPC2 in the context of other programs; consequently, we were not allowed to ‘duplicate’ the optical observations for these 9 systems. The archival images for these galaxies, however, were not taken in the F606W filter which we had chosen for our own WFPC2 survey. Given the arbitrary assumptions that would underlie the conversion from the “archival”-F160W into the F606W-F160W color (a conversion necessary for studying these systems together with the other objects of our sample), we have not included these 9 galaxies in the statistical study presented in this paper, to guarantee the homogeneity of the results. The  $H$  images of these systems at HST resolution are presented in Appendix A. The remaining 69 objects are considered in this study. At the time of the NICMOS Phase II submission, no WFPC2 data were available either in the archive or as part of our snapshot program for 46 of the targets. For these objects a F110W image was also included in our NICMOS observing plan; 41 of these 46 systems were actually observed in our NICMOS survey with both the F160W and the F110W filter. These F110W and F160W exposures consist of two MULTIACCUM sequences with STEP256 and NSAMP=10, for a total exposure time of 256 seconds per filter. For 30 of these 46 galaxies WFPC2

F606W images were obtained, as part of our WFPC2 snapshot program, after the NICMOS phase II deadline. Thus, images in the three filters F606W, F110W and F160W, are available for these 30 systems. For the remaining targets F606W WFPC2 images were already in hand at the time of the NICMOS phase II deadline. For these objects we acquired three F160W MULTIACCUM sequences with STEP256 and NSAMP=10, which results in a total exposure time of 384 seconds. Images in both F160W and F606W are available for a total of 58 galaxies. Table 1 lists the 69 galaxies considered in this study together with the list of filters in which they have been observed, the galaxy distance in Mpc, morphological type, apparent total  $B$  magnitude,  $B$  extinction, as well as the information on whether an  $R^{1/4}$  or an exponential bulge is present, and the type of central spectrum observed at ground-based resolution.

for these objects, including whether they were also observed within our program in F110W and/or in F606W.

The NICMOS images were reduced with the standard pipeline software, using the on-orbit flats and darks identified in the HST archive as the best-reference frames. The various NICMOS image-anomalies were corrected on a case-by-case basis. All images were affected by the so-called ‘pedestal’ anomaly, a time-variable bias of unclear origin. In most of the images the pedestal was removed using the NICMOS Pedestal Estimation Software (developed by R.P. van der Marel). In about 10% of the images the pedestal effects were very severe, and they had to be removed iteratively. In some galaxies (ESO240G12, ESO404G3, ESO443G80, ESO548G29, ESO549G18, ESO572G22, IC1555, NGC1345, NGC1800, NGC3455, NGC4806, NGC4980, NGC7188 and NGC7241), even after removal of the pedestal, a constant gradient across the chip remained visible. This was removed by subtracting a linear fit to the edges of the chip, using the ‘imsurfit’ routine in IRAF. In about 30% of the images additional anomalies such as shading and bias jumps/bands were present. These were also removed from the images before performing the measurements.

The combined images were flux-calibrated adopting the pipeline flux calibration zeropoints,  $ZP_{F110W} = 23.248$  for the F110W filter and  $ZP_{F160W} = 23.110$  for the F160W filter (AB system, Oke & Gunn 1983). Magnitudes for our WFPC2 data were originally given in “Vegamag”; we

converted them to the AB system by using  $V_{606,AB} = V_{606,Vega} + 0.117$ . The conversion between AB and Vegamags was computed by us using the Synphot synthetic photometry package (in IRAF) with the spectrum of Vega as input.

$V - H$  color maps were derived for the NICMOS galaxies for which WFPC2 F606W images were also available, including 8 objects for which the optical images were obtained after the publication of the WFPC2 results (asterisks close to the galaxy name in Table 1). To account for the difference in Point Spread Function (PSF) between the  $H$  and  $V$  images, the images in a given band were convolved with the PSF of the other band. All PSFs were obtained with TINYTIM (Krist 1997). The adopted extent of the PSF images generated by TinyTim was  $3''$ . The PSF FWHM was  $0.127''$  for the F160W filter, and  $0.091''$  for the F110W filter, respectively; a  $5 \times 5$  sub-pixel scale was used. The  $V$  and  $H$  images were aligned after sub-pixel rebinning before computing the color maps. For the 11 galaxies for which the only additional images available were those in the F110W filter, we computed the  $J - H$  color maps following the same approach just described for the optical-NIR maps.

The identification of the nuclei in the NIR images was based primarily on visual inspection of the images, and was checked on the radial light profiles for those systems for which an isophotal fit could be derived (paper II). Similar to what was done for the visual WFPC2 data, the nuclei were selected based on the criterion that their compact, smooth, regular-morphology excess of light was well-isolated from the remaining circum-nuclear structure. In Figure 1 a we show the  $H$  images and  $V - H$  color maps for 38 of the 39 galaxies that host a distinct nucleus and that were imaged both in F160W and F606W (the image of the 39th object, ESO549G18, had a S/N sufficient for measuring the parameters of the nucleus, but not for studying the underlying galaxy); in Figure 1 b we show instead the  $H$  and  $J - H$  images for the 5 galaxies which host a distinct nucleus for which the only other filter available in addition to F160W is F110W. Figures 2 a and b show the similar images for those galaxies which either do not host a distinct nucleus, or in which the presence of a nucleus is uncertain. In Figures 3 a and b we show the  $H$ -band light profiles of two galaxies representative of the two subsets presented in Figures 1 and 2, respectively: the



first galaxy hosts a distinct nucleus embedded in an exponential pseudo-bulge (panel a; NGC 2082); the other galaxy hosts an  $R^{1/4}$ -law bulge (panel b; NGC 2460). In the NGC 2082 the photometrically-distinct nucleus is clearly identifiable in the  $H$  light profile inside the innermost few tenths of arcsecond, similarly to what was found in the visual band. In contrast, in the NIR as in the  $V$  band, the  $R^{1/4}$ -law bulge shows the steep luminosity profile typical of this class of objects (Carollo et al. 1998; Carollo & Stiavelli 1998; paper II).

## 2.2. Radii and Luminosities of the Nuclei in the NIR

The NIR measurements of the magnitudes and radii of the nuclei are affected by the uncertainty on the light contribution from the underlying galaxy. To quantify the luminosities of the nuclei in the NIR we adopted the three approaches previously optimized to extract similar information from the **WFPC2** visual images, namely: (1) we fitted the contribution from the nucleus with a Gaussian, assuming that the underlying galactic light continuum is well represented by the asymptotic value of the Gaussian wings; (2) we modeled the underlying galactic light with a fourth-order polynomial using the task “fit/flat” in **ESO/MIDAS**, subtracted this model from the image, and attributed the excess counts to the nucleus; (3) we subtracted from the original frame an iteratively smoothed and nucleus-masked version of it, and performed the measurement on the resulting image containing only the nucleus. These three methods are complementary: they sample the galactic background in different regions, and hence their combined use allows us to estimate the uncertainty in the derived values contributed by the poorly constrained underlying galactic light. As done for the optical measurements, we adopted as final the averages of, and as errorbars the mean of the differences between, these three estimates for the luminosity of the central sources. The sizes of the compact sources were taken equal to the FWHM of the best fitting Gaussians of method (1), corrected for the instrumental width of **NICMOS** assuming that the intrinsic profile of the nucleus is described by a Plummer law (see Eq. 2). Consistent with the **WFPC2** study, in the following we adopt for the half-light radii of the nuclei the ratio between half-light radius and FWHM valid for

a Plummer law (see below). This gives a better representation than, e.g., a Gaussian shape, given that all compact sources show wings in excess of a Gaussian. An assessment of the systematic uncertainties associated with the adopted radii and luminosities of the nuclei is given in Appendix B.

In our WFPC2 study of the nuclei (Carollo et al. 1997; Carollo et al. 1998), for those galaxies with an isophotal/analytical fit available, we also estimated the magnitudes and luminosities of the nuclei by using two additional approaches: *(a)* We adopted the best fitting (exponential) models of the bulges to describe the underlying galaxian light, subtracted these models from the images, and attributed the residual nuclear counts to the nuclei; *(b)* We fitted the entire radial light profiles, including the innermost points, with multi-component analytical laws representing the bulge with an exponential law and the nucleus with either an  $R^{1/4}$ -law, or a Plummer law, or a modified Hubble profile. These alternative approaches provided results in agreement with—and well within the range spanned by—those obtained using the methods (1), (2), and (3) discussed above. To guarantee a homogeneous and self-consistent set of measurements, however, in our WFPC2 analysis we only used the results obtained from the latter three methods, since the additional two approaches could only be applied to a subset of the sample. Due to the limited radial extension of the NICMOS data, no bulge/disk decomposition was performed on the NIR data, and therefore no exponential fits are available for the bulges in  $H$  or  $J$ . Thus, these additional tests could not be performed on the NIR profiles. Nonetheless, the results of the tests conducted on the WFPC2 data give us confidence that also for the NICMOS measurements the error bars derived from the “primary” methods (1), (2) and (3) do reliably represent the uncertainty associated with disentangling the unknown contribution from the underlying galaxy.

Finally, we computed the location of the nuclei by measuring their centroids, and the centers of their host galaxies by measuring the centers of the isophotes computed at  $\approx 1''$  (the precise radius was slightly increased/decreased in some galaxies to avoid the effects of prominent structures). The elongation of the nuclei was established by visual inspection.

### 3. Results and Discussion

#### 3.1. The Central Regions of Spirals in the NIR

A large structural complexity is observed in the  $H$  band in the central regions of many spiral galaxies; on the other hand, it is clear that the NICMOS images provide a much cleaner picture of the underlying galaxy structure as compared to the heavily dust-obscured WFPC2 visual images. In the extreme cases of NGC 3067, NGC 4750 and NGC 6239, the NICMOS images unveil the location of the true galaxy center, which we had been unable to identify in the WFPC2 images due to strong dust features and star formation. The NICMOS images have revealed in two of these galaxies (NGC 4750 and NGC 6239) the presence of a distinct compact nucleus, which subsequently, with the acquired knowledge of its precise location, we have been able to identify and parametrize also in the WFPC2 images. The optical measurements for these nuclei were not reported in our previous papers; these measurements are reported here in Table 2, identified by the “†” symbol. The possibility of better “penetrating” the dust in the NIR with respect to the optical data has also led to the identification, based on the visual inspection of the  $H$  images, of nuclear bar-like features in ESO499G37, NGC 4384, NGC 4750, NGC 5448, NGC 5806, NGC 7280 (identified by ‘S’ —standing for small— in the column ‘Bar’ in Table 3), and possibly also in IC4390, IC 5271, IC 5273, NGC 289, NGC 2339, NGC 3455, NGC 3898, NGC 3949, NGC 4102, NGC 4219, NGC 4806, NGC 5678, NGC 6810, NGC 7177, NGC 7188 and NGC 7690 (these ambiguous cases are identified by ‘S?’ in Table 3). In IC 4390, IC 5271, NGC 3455, NGC 3949, NGC 4219, and NGC 5448 the nuclear bar-like features become evident in the  $V - H$  or  $J - H$  maps by their distinct colors (either redder or bluer than the surroundings). Consistent with the studies which have looked for nuclear bars in the context of the feeding of an active non-thermal nucleus, we find that even in the less dust-sensitive NIR images the nuclear bar-like features are not ubiquitous. Interestingly, spiral structure down to the center/nucleus is observable in the  $H$ -band images of several systems. In some galaxies, ESO205G7, NGC3928, NGC5678, a small-scale ring is observed around the centre/nucleus; these rings are likely not an artefact of PSF mismatch (since changing

the sizes of the PSFs by 10% does not affect the result), and are likely due to circum-nuclear dust or star formation.

In summary, the NIR images, coupled with the optical images, show that there is no galaxy in our sample that is not “polluted” either by dust or by recent star formation or both in its nuclear/circum-nuclear region: all galaxies contain some nuclear/circum-nuclear feature overlying the smooth/old stellar populations. Excluding a few objects for which the signal-to-noise ratio of the NIR images is too low to accurately measure the underlying light outside the bright nucleus, the galaxies in our sample can be broadly grouped into a four classes, based on their nuclear NIR- and optical/NIR-color morphology:

*Class 1. Galaxies with Concentrated Nuclear Star Formation Mixed with Dust.* Judging from the  $H$  images and the optical-NIR color maps, many galaxies (ESO 498 G5, ESO 499 G37, IC 4390, IC 5273, NGC 406, NGC 986, NGC 1483, NGC 1688, NGC 1800, NGC 2082, NGC 2566, NGC 2964, NGC 3067, NGC 3928, NGC 4102, NGC 4219, NGC 4384, NGC 5678, NGC 5806, NGC 6000, NGC 6329, NGC 6951, NGC 7217, NGC 7259) host in their innermost few-hundred pc<sup>2</sup> concentrated star formation in the form of compact blue knots, intermixed with strong red dust features. With the exception of NGC 2566, NGC 3928, NGC 7217, and NGC 7259, where the star forming and dust features have a regular spiral morphology, and of NGC 6951, where they form a circum-nuclear ring, in all the remaining objects the nuclear star formation and dust have a rather irregular morphology. Only some of these systems have been found to host a nuclear bar or a central nucleus, so that the presence of these features is not a unique characteristic of this family of objects. All but four (ESO 499 G37, IC 5273, NGC 1688, NGC 1800) of these galaxies are early-to-intermediate type spirals in the Hubble range between Sab and Sbc. From these data it seems that star formation in the central regions of early-type spiral galaxies does not occur in the rare, transient, and intense “starburst mode”: low-level star formation appears to be common in these systems. A question to answer is whether this low-level star formation represents the low-luminosity end of the starburst phenomenon, or rather the fading evolutionary descendant of a major starburst itself (Heckman 1997).

*Class 2. Galaxies with Diffuse Blue Nuclear Regions.* Several systems, namely ESO 240 G12, NGC 972, NGC 1345, NGC 1398, NGC 2339, NGC 2748, NGC 3949, NGC 4527, NGC 5188, NGC 5377, NGC 5448, NGC 6810, NGC 7177, and NGC 7690 also host significant amounts of circum-nuclear dust mixed with rather blue surroundings; the latter however have a more diffuse appearance than the knot-like features typical of the previous group. For example, in NGC 5377 the blue region is embedded in a completely-obscuring dust torus and has the morphology of regular disk surrounding the distinct central nucleus. Among these systems there are a few (NGC 5377, NGC 5448, NGC 6810) which are known to host an AGN; for them, it is possible that the blue regions are related to non-thermal activity from the central engine.

*Class 3. Galaxies with Regular Nuclear/Circum-Nuclear Dust.* There are some galaxies that do not show evidence for star formation (with the possible exclusion of the nucleus), but host in their central regions strong dust lanes with a regular, well-defined spiral or ring morphology. These systems are ESO 205 G7, NGC 488, NGC 772, NGC 2460, NGC 3259, NGC 3277, NGC 4750, NGC 6384, NGC 7013. Some of these objects show some ionized-gas emission on ground-based scales (Table 1), but this must be distributed smoothly in the central region not to show up clearly in the images in the form of identifiable structures. Apart from being all early-to-intermediate type systems (S0a to Sbc), these galaxies show no other characterizing feature: some belong to the group of Figure 1 and thus host a distinct nucleus, others belong to the group of Figure 2; some have an exponential bulge, others host instead an  $R^{1/4}$  bulge. The nuclei which are embedded in some of the galaxies in this class tend to have relatively red  $V - H$  colors, ranging from 1.3 to 2.1 magnitudes.

*Class 4. Galaxies with Irregular Nuclear/Circum-Nuclear Dust.* Several more objects in the sample also show a quiescent, non-starforming morphology with strong dust features, but the latter are distributed in a much more irregular and patchy way (although in some cases, in addition to the irregular patches, spiral-like dust is also present). These objects are IC 5271, NGC 289, NGC 1892, NGC 2196, NGC 2344, NGC 2758, NGC 3455, NGC 3898, NGC 3900, NGC 4806, NGC 4980, NGC 5985, NGC 6340, NGC 7162, NGC 7188, NGC 7280, NGC 7421, NGC 7513. Similar

to the case above, some of these systems host a central distinct nucleus, others do not; with the exception of NGC 1892, they are early-to-intermediate type systems, with Hubble types between S0 and Sc. The  $V - H$  colors of the four nuclei detected in this class of systems range from 1.4 to 3.1 magnitudes; the latter high  $V - H$  value clearly indicates the presence of a significant amount of dust even on the nucleus itself. In several of these systems the presence of a nucleus is uncertain, due to the dust which obscures the central region.

Additional information is concisely reported in Table 3 where we summarize, object by object, the observed properties of the circumnuclear  $V - H$  or  $J - H$  light distribution.

### 3.2. The Nuclei

Table 2 lists the F160W sizes and luminosities for the nuclei detected in the NICMOS sample, measured as described in §2.2. When available, the sizes and luminosities of the nuclei in the F110W passband are also listed, together with, for an easy comparison, the F606W measurements published in Carollo et al. (1997, 1998) for the NICMOS galaxies observed within our program also with WFPC2. The F606W properties of the nuclei for the 8 NICMOS targets which were not included in our WFPC2 papers due to the late acquisition of the WFPC2 images (§2.2) are also given in the Table. The comparison of the sizes derived from the WFPC2 and F110W images with those derived from the F160W images is shown in Figure 4. The radii measured with NICMOS and WFPC2 are in good agreement within the error bars.

Compact star-cluster-type nuclei in bulgeless, weakly- or non-active late-type disks have been the subject of a few detailed studies (Kormendy & McClure 1993; Phillips et al. 1996; Matthews & Gallagher 1997; Lauer et al. 1998). In the visual band, these late-type nuclei have been found to cover a very narrow range in luminosity ( $M_I \sim -11 \pm 1$ ) despite the large range in luminosity of their host galaxies (from  $M_V = -15.1$  to  $M_V = -18.2$ ; Matthews et al. 1999). Our WFPC2 and NICMOS surveys show that photometrically-distinct nuclei are very frequent also in

intermediate-type spirals. In contrast with the four nuclei in our sample embedded in the late-type galaxies, which lie typically ‘naked’ in the centers of the disks (as reported also by Matthews et al. 1999), in the earlier-types the nucleus is embedded either in a smooth pseudo-bulge with an exponential radial light profile, or, in the case of the brightest nuclei ( $-12 \gtrsim M_V \gtrsim -16$ ), in a complex structure of strong dust lanes and star-forming knots in irregular, spiral or ring-like patterns typically still observable also in the NIR (see also Carollo et al. 1997; Carollo et al. 1998; Devereux et al. 1997). Furthermore, the new data show that:

(i) Within our sample, in all cases for which a nucleus was detected in the WFPC2 images and for which the NICMOS data are available, the nucleus is also clearly seen in the NIR: this suggests that all nuclei, independent of Hubble type, are relatively massive, given that the NIR light around  $1.6\mu$  is a rather good tracer of the stellar mass. In the NIR as much as in the visual passband, however, the nuclei embedded in the bright early- to intermediate-type hosts span a much larger magnitude range than the nuclei embedded in the fainter late-type disks, as shown in Figure 5 a, where the absolute  $H_{AB}$  magnitude of the nuclei is plotted against their half-light radius derived in the same passband: The four nuclei embedded in the Scd and later-type disks have nuclear properties quite similar to those reported in the quoted literature for other late-type nuclei, and are therefore likely representative of that category of objects.

(ii) In our sample we find nuclei that are either embedded (e.g., NGC 6000) or not embedded (e.g., NGC 2964) in large-scale ( $\gtrsim 1$  kpc) bars. We also find that some of the nuclei sit within smaller bars, with scales of up to a few 100 pc (e.g., ESO499G37). These small-scale bars could be particularly important within the context of bar-driven secular evolution scenarios for bulge formation, since they might provide a mechanism for bringing the disk material from the outer regions down to the pc scales in the shallow gravitational potential of the progenitor disks (Shlosman 1994; Shlosman & Robinson 1995; Shlosman, Begelman & Frank 1990; Friedli & Martinet 1993). The nucleus/nuclear-bar connection is however not a straightforward one since, as stressed above, nuclear bars are not a universal feature of nucleated spiral galaxies.

(iii) The brightest nuclei embedded in the early/intermediate-type galaxies tend to have

larger radii than the fainter nuclei. An increase of radius with increasing luminosity of the compact nucleus in the early/intermediate types is detected in the  $H$  band (linear correlation coefficient of -0.76, corresponding to a probability  $> 99.9\%$ ). This was already noticed in the F606W passband (see Figure 5 b, where the absolute magnitude versus half-light radius relation for the nuclei is given for the  $V$  band, for a comparison with Figure 5 a, where the same relation is given the  $H$  band). The same finding in the NIR, however, strengthens the reliability of this result, given the much simpler circumnuclear background structure in the  $H$  band as compared to the complex one in which (especially the brightest) nuclei were found embedded in the visual images. The measurements of the half-light radii of the nuclei have a rather large uncertainty, mostly because at the distance of our sources the extended light component of the nucleus must be separated from the wings of the PSF (see also Matthews et al. 1999). The galaxies of our sample are however restricted to  $cz < 2500$  km/s, which ensures a rather high degree of homogeneity in the derived set of measurements. In contrast with the simulations, which showed a modest brightening of the nucleus corresponding to a modest increase in radius, the nuclei observed in the centers of early/intermediate-type spirals span an entire decade in radius, over which they show an increase in luminosity of about eight magnitudes. It is therefore likely that a substantial part of this correlation is driven by a real physical effect.

(iv) The resolution of the data is not appropriate to detect color variations within individual nuclei, but it is adequate to compare the nuclei to their surroundings. The early/intermediate-type spirals' nuclei are found to cover a large range of colors, from  $V - H \approx -0.5$  to 3. Previous HST studies on the colors of the central regions of spirals report very red (dusty) centers for the early-type bulges (Peletier et al. 1999), and rather blue colors for the distinct nuclei of late-type disks (Matthews et al. 1999). The few late-type nuclei in our sample show a slight tendency for having bluer colors than the nuclei of the earlier-type hosts, as is shown in Figure 6, where the  $V - H$  color of the nuclei is plotted against the RC3 Hubble type of the host galaxy. Figure 6 also shows however that the spread in  $V - H$  color is rather large within the early/intermediate types themselves: The early/intermediate nuclei have an average  $V - H \approx 1.44$  with a sigma of about 0.82 magnitudes. In the Figure, the nuclei are identified with different symbols according to the



galaxy-class to which their hosts belong (among the four described above; symbols are explained in the figure caption). No significant trend is observed with galaxy-class, with only a possible hint for the nuclei embedded in galaxies with regular nuclear/circum-nuclear dust to be slightly redder than the average. A comparison of each nucleus with its own galactic surroundings shows that the nuclei are in some cases redder and in others bluer than their hosts (see Table 3, where we also provide a summary of the properties of the nuclei in the  $H$  band, and of their optical-NIR or NIR-NIR color properties). Statistically, the distribution of  $V - H$  colors is broader for the nuclei than for the surrounding galactic structure, as seen in Figure 7 which compares the  $V - H$  color distribution for the nuclei with the  $V - H$  color of the host galaxies. This Figure contains only those galaxy-nucleus pairs for which an isophotal fit to the underlying light of the host galaxies in both the  $V$  and the  $H$  band could be performed, so that their  $V - H$  color could be derived by integrating the  $V$  and  $H$  radial light profiles within  $3''$  (see Carollo & Stiavelli 1998 and paper II for the  $V$  and  $H$  fits, respectively). The so-obtained colors are much less affected by the effects of dust or recent star formation with respect to aperture measurements. No isophotal fit could be performed for the hosts of some of the nuclei of Figure 6, and in particular to the hosts of the reddest and bluest nuclei; this explains the smaller range in  $V - H$  of Figure 7 with respect to Figure 6. Even so, the Kolmogorov-Smirnov, Kendall and Spearman tests give a probability of 0.996, 0.999 and 0.9997 that the two distributions are statistically different. This likely indicates ubiquitous presence of either ‘activity’ or dust reddening (or both) in the nuclei population. Figure 8 a shows the  $V$  absolute magnitude versus the  $V - H$  color for the nuclei; Figure 8 b shows their  $J - H$  versus  $V - H$  color-color diagram. Different symbols in these Figures (are as in Figure 6 and) are used to identify nuclei embedded in hosts belonging to a different galaxy-class among the four discussed above. A more detailed discussion of these color-magnitude and color-color diagrams, and in particular of the constraints that they put on the stellar population properties of the nuclei, is given in Carollo et al. (2001); what we remark here is that there is no obvious trends for any ‘segregation’ on these diagrams among nuclei embedded in hosts with different circum-nuclear properties.

(v) Within the caveats imposed by the angular resolution of our data and the distance of

our targets, no significant difference is found with Hubble type concerning the exact location of the nuclei with respect to the underlying galactic structure, and their projected shape, round versus elongated. In Table 3 we report, for each galaxy, whether the compact nucleus is centered on, or offset from, the galaxy isophotal center, and whether the nucleus and more generally the nuclear region is round or elongated. There are several cases where our NICMOS data suggest that the nuclei are not located precisely at the isophotal centers of the host galaxies, as found e.g. for M33 (de Vaucouleurs & Freeman 1970; Minniti et al. 1993). There are also a few cases where the nucleus shows some degree of elongation, as also found for, e.g., the nucleus of M33 (Kormendy & McClure 1993; Lauer et al. 1998; Matthews et al. 1999). With the current data, the displacement and elongation, however, appear not to be correlated with either the luminosity and color of the nucleus, or the galaxy type. It remains an open issue whether some nuclei are disk-like features, and whether the nuclei of galaxies with an AGN are intrinsically different from those of non-AGN galaxies. On the other hand, the fact that many of the best-resolved nuclei are typically round structures in projection supports the working hypothesis that (at least in non-AGN galaxies and) for all Hubble types these nuclei are typically cluster-like systems.

#### 4. Summary

We have presented the analysis of HST NICMOS data in the F160W ( $H$ ) filter for the central regions of a sample of 78 mostly early-to-intermediate type spiral galaxies. For 58 of these systems we have used WFPC2 F606W ( $V$ ) images from our previous study to investigate their  $V - H$  nuclear colors. For 11 systems we have used additional NICMOS images in the F110W filter to investigate their  $J - H$  nuclear colors. We have focused our attention on the structural and color properties of the photometrically-distinct nuclei that (similarly to what we had previously found in the visual band) dominate the nuclear light in a large fraction of the sample in the NIR, and on their galactic circum-nuclear regions.

Although the nuclear complexity that was unveiled in many of these galaxies by the WFPC2

images is often still present in the  $H$  band, the latter provides a cleaner view of the nuclear galactic structure, and allows to see through areas of recent star formation and through dust patches typically present in the central regions of these system. This strengthens the findings which we had previously suggested on the basis of our HST optical images, and adds further clues for understanding the nature and origin of galactic nuclei. In particular, several nuclear bar-like features have been detected in the  $H$ -band, including some which have a  $V - H$  or  $J - H$  color distinct from that of their surroundings. Nuclear bars are however not ubiquitous in this kind of systems. Any relation between the presence of a nucleus and of a barred component, if present, is not a simple one, as nuclei are found in both barred and non-barred hosts. In the  $H$  band, consistent with what was found in the  $V$  band, the nuclei embedded in the bright early- to intermediate-type hosts span a much larger magnitude range (about eight magnitudes) peak-to-peak than the nuclei embedded in the fainter late-type disks. In the  $H$  band, the brighter the nucleus the larger its radius, a correlation that was found in the  $V$  band and is confirmed by the NIR data. Even excluding the few bluer-than-average late-type nuclei in our sample, the nuclei of early- to intermediate-type spirals span a large range in  $V - H$  colors, some being significantly redder (and very likely dust-reddened), others being significantly bluer (‘polluted’ either by a non-thermal component or by recent star formation), than their surrounding circumnuclear regions. Several nuclei embedded in the early- to intermediate-type hosts are offset (typically by a few tens of pc) from the isophotal centers of the host galaxies; several are flattened structures; however, most of the nuclei, at HST resolution, are located at the galaxy centers, and appear to be round, cluster-like structures.

A quantitative analysis of the circum-nuclear galaxy structure and strength of the nuclear stellar cusp slopes in the NIR is reported in paper II.

We thank Roeland van der Marel for providing the pedestal-removal software, and the anonymous referee for his/her careful review that has helped us improve the presentation of our results. This research has been partially funded by Grants GO-06359.01-95A and GO-07331.02-96A

awarded by STScI, and has made use of the NASA/IPAC Extragalactic Database (NED) which is operated by the Jet Propulsion Laboratory, Caltech, under contract with NASA.

### Appendix A. NICMOS $H$ Band Imaging for Nine Galaxies

In Figure 9 we present the NICMOS F160W images of the nine galaxies in our sample for which neither WFPC2 F606W nor F110W images are available. The data reduction was done as described in §2. NGC1365 (a well-known AGN), NGC2903, NGC3031, NGC4569, and NGC6217 host photometrically-distinct nuclei; NGC 4569 also hosts a nuclear disk. The presence of a nucleus is uncertain in NGC4536 and NGC4565; no nucleus is present in NGC7479 and NGC7742. Table 4 summarizes some properties of the nine galaxies, including the  $H$  measurements of sizes and magnitudes for the nuclei.

### Appendix B. Assessment of Systematic Effects

Measuring the half-light radius and luminosity of a distinct nucleus embedded in a galaxy core entails assumptions on how to partition the observed light between the underlying galaxy and the nucleus. The different assumptions that we have used in §2.2, while all yielding acceptable decompositions, provide however different results, since it is not easy to establish where the nucleus ends and the galaxy begins. The situation is therefore one where the systematic error arising from separating the galaxy light from the nucleus light outweighs the error on the measurement of the radius and the luminosity of the nucleus itself. To assess the systematic errors on these quantities, we performed two sets of tests. The results for the F160W filter are described below. A similar analysis was performed for the F110W and the WFPC2 F606W filters, reaching similar conclusion as for the F160W filter.

First, we tested the sensitivity of our nucleus-extraction procedure in the region of parameter space covered by those nuclei embedded in hosts for which an isophotal fit could be performed,

and whose nuclear surface brightness profiles could be modeled with a Nuker-law (Lauer et al. 1995; see paper II for the description of our isophotal and Nuker fits). The Nuker law reduces to a power law when the characteristic radius  $r_b$  is much larger than the nucleus’ radius. We built model galaxy images starting from the best-fit analytical descriptions of the light underlying the nuclei in these galaxies, and added to each of these model galaxies a contribution from a nucleus of size and luminosity equal to those measured with our procedure in that specific system. Two different analytical forms were adopted to describe the nuclei, a “generalized” modified-Hubble law, which reads:

$$I(R) = \frac{L}{2\pi b^2} \left( 1 + \frac{R^2}{b^2} \right)^{-5/2} \quad (1)$$

and a Plummer law, which reads:

$$I(R) = \frac{L}{b^2} \left( 1 + \frac{R^2}{b^2} \right)^{-2}. \quad (2)$$

In both Eq. (1) and (2)  $b$  is the scalelength and  $L$  is the total luminosity. We then convolved the model galaxy-plus-nucleus images with the NICMOS PSF in the appropriate filter (obtained with TINYTIM, as done for the data), and applied our nucleus-extraction procedure to these PSF-convolved model-images. The radius was corrected for PSF broadening in the same way as was done for the actual data. This test provides an estimate of how accurately we can disentangle the nuclei from their hosts for galaxy-plus-nucleus pairs of the kind that we have detected (similar sizes/luminosities of the clusters; similar contrasts with the underlying/surrounding galaxy).

Figures 10 a and b show, for these galaxy-nucleus pairs, the distribution of the ratio between the recovered flux and the input flux, and the distribution of the ratio between the recovered radius and the input radius, respectively. Figure 10 c shows  $\Delta mag = (m_{recover} - m_{input})$ , the difference between the recovered and the input magnitude, as a function of the logarithm of the ratio between recovered and input radius (after correction for systematic shifts). The figures show that 90% of the measurements lie within  $\approx 0.3$  magnitudes from the expected values, and that our extraction procedure applied to the intrinsic nuclear light profiles systematically underestimates

the flux on average by  $\approx 0.4$  magnitudes, with a scatter of  $\approx 0.2$  magnitudes. By contrast, the mean radius appears to be overestimated in average by  $\approx 45\%$ , with a scatter of  $\approx 25\%$ ; the 50%-error includes  $\approx 80\%$  of the points. A weak correlation between the derived radius and magnitude of the nuclei is detected, but the maximum absolute variations are rather modest, about a factor 3 increase in radius for a  $\approx 1$  magnitude brightening of the nucleus.

Secondly, we performed another set of tests which covered a larger area of parameter space to assess the degree of degeneracy in the parameters provided by our galaxy-nucleus decomposition. These additional tests allow us to estimate how much and often intrinsically different galaxy-nucleus pairs can result in similar measurements when analysed with our procedure. We built a grid of model galaxies described by either a power-law cusp of slope  $\gamma$  ranging from 0 to 0.7, or an exponential profile, and we added to these model galaxies the contribution from a central nucleus, described by a Plummer law. The nucleus was assumed to have  $H_{AB} = 19.6$ ; the surface brightness of the underlying galaxy was taken similar to the typical one observed for real objects. In particular, a mean  $H_{AB}$  surface brightness within  $20''$  equal to  $19.7 \text{ mag/arcsec}^2$  was considered for the power-law galaxies, corresponding to a central surface brightness after convolution with the PSF of 19.2, 18.4, 17.4 or  $16.4 \text{ mag/arcsec}^2$  for  $\gamma = 0.1, 0.3, 0.5$  or  $0.7$ , respectively. For the two highest  $\gamma$  values of 0.5 and 0.7, also a mean surface brightness within  $20''$  equal to  $20.5 \text{ mag/arcsec}^2$  was considered, corresponding to a central surface brightness after convolution with the PSF of 18.2 or  $17.2 \text{ mag/arcsec}^2$ , respectively. A central surface brightness equal to 18.5 or  $19.3 \text{ mag/arcsec}^2$  was considered instead for the exponential galaxies. We convolved this set of galaxy-nucleus models with the appropriate PSF, and applied our procedure to recover the input parameters.

Figure 11 a shows the  $\Delta mag$  (the difference between the recovered and input  $H_{AB}$  magnitude of the nucleus) versus the nuclear cusp slope  $\gamma$  for the power-law galaxies, and versus the exponential scale-length for the exponential galaxies. Figure 11 b shows the recovered- versus the input-FWHM of the central nucleus. Notice how difficult it is to recover the radius of the nucleus when a large nucleus lies on top of an underlying steep cusp. Figure 11 c shows the

$\Delta mag$ , the difference between the recovered and the input magnitude, versus the recovered radius of the nucleus. The results of this set of tests demonstrate that when all the galaxy-nucleus pair models are taken into account, the flux is underestimated by  $\approx 0.27$  magnitudes, with a scatter of 0.60 magnitudes; 80% of the points lie within the 50% flux error. The radius appears to be overestimated by  $\approx 30\%$  with an rms of  $\approx 40\%$  and with the 50%-error including 90% of the points. Also these general models - especially the power-law ones - show a weak trend between derived radius and magnitude of the nuclei. The observed maximum variation is again about a factor 3 of increase in radius, which in this case corresponds to  $\approx 1.5$  magnitude brightening of the nucleus.

Summarizing, both the tests performed on specific galaxy-nucleus pairs and the more general ones indicate that: (1) the reported fluxes are likely underestimated by  $\approx 0.3$  magnitudes, and are accurate to better than 0.6 magnitudes; (2) the reported radii are likely overestimated by about 40% and are accurate to within 40%; (3) the galaxy-nucleus degeneracy and possibly the adopted extraction technique may produce a mild trend for brighter nuclei to be slightly more extended than fainter nuclei, although it is unlikely that such an artifact could produce a correlation between luminosity and size of the nuclei involving several magnitudes of difference in luminosity.

We finally checked whether there was any major systematic effect affecting our measurements depending on the luminosity of the nucleus embedded in a given galaxy. We computed an additional set of about 200 galaxy-models with a central surface brightness of  $18.4 \text{ mag arcsec}^{-2}$  and nuclei with a range of luminosities; we used both power-laws and exponentials models with cusps and exponential lengths covering the same intervals as in the models of Figure 10. While the systematic error in the measurement increases, there is no systematic trend on the recovered luminosity of the nucleus. This is illustrated in Figures 12 a and b where we plot, as a function of the input magnitude of the nucleus, the difference between the recovered and the input magnitudes for both power-law and exponential galaxy-models, respectively. For each luminosity bin the plot shows the mean shift and the error; the latter is dominated by systematic effects.

Although these experiments do provide an estimate of the size of our systematic errors, we have chosen not to apply these “corrections” to the radii and luminosities of the nuclei in

our analysis, since: *(i)* the absolute amount of the systematic shifts is not such to affect in any significant way our conclusions, and *(ii)* the estimated correction would be strictly valid if all nuclei were “homologous”, i.e., had similar intrinsic profiles, and could instead introduce additional scatter if the intrinsic light profile changed from nucleus to nucleus.

The combined results for the WFPC2 and NICMOS tests were used to assess the uncertainties associated with the colors of the nuclei. On the assumption that nuclei and underlying galaxies have similar intrinsic light profiles in the visual and NIR and do not have large unresolved color gradients, the same analytical models would properly describe both the  $V$  and the  $H$  band data. In this case one expects the error on the  $V - H$  color of the nuclei to be much smaller than the total formal error obtained by quadratically adding the errors on each band. We checked this assumption on the galaxy-nucleus pairs of Figures 10 a and 10 b. In Figure 13 we show the histogram of the error on the  $V - H$  color obtained adopting for the nuclei a modified Hubble profile (solid line) or a Plummer law (dotted line): The figure shows that although the systematic effect is not entirely cancelled, the resulting error is reduced to 0.4 magnitudes instead of the formal 0.8 magnitudes.



## REFERENCES

- Bureau, M., Freeman, K., 1999, AJ, 118, 126
- Burstein, D., & Heiles, C., 1984, ApJS, 54, 33
- Carollo, C.M., Stiavelli, M., de Zeeuw, P.T., Mack, J., 1997, AJ, 114, 2366
- Carollo, C.M., Stiavelli, M., Mack, J., 1998, AJ, 116, 68
- Carollo, C.M., Stiavelli, M., 1998, AJ, 115, 2306
- Carollo, C.M., 1999, ApJ, 523, 566
- Carollo, C.M., Stiavelli, M., de Zeeuw, P.T., Seigar, M., Dejonghe, H., 2001, ApJ, 546, 216
- Courteau, S., de Jong, R. S., Broeils, A. H., 1996, ApJ, 457, L73
- de Vaucouleurs G., de Vaucouleurs A., Corwin H. G. Jr., Buta R. J., Paturel G., Fouqué P., 1991,  
Third Reference Catalog of Bright Galaxies, (New York: Springer Verlag) (RC3)
- de Vaucouleurs G., Freeman, K., 1970, in “The Spiral Structure of Our Galaxy”, IAU Symposium  
no. 38, Dordrecht, Reidel, p. 356
- Devereux, N., Ford, H., Jacoby, G., 1997, ApJ, 481, L71
- Friedli, D., Benz, W., 1993, AA, 268, 65
- Friedli, D., Martinet, L., 1993, AA, 277, 27
- Hasan H., Pfenniger D., Norman C., 1993, ApJ, 409, 91
- Heckman, T., 1998, ASP Conference Series, Vol. 148, eds. C. E. Woodward, J. M. Shull, and H.  
A. Thronson, Jr., p. 127
- Ho, L.C., Filippenko, A.V. & Sargent, W.L., 1997, ApJS, 112, 315
- Kormendy J., 1993, IAU Symposium 153, Galactic Bulges, eds H.J. Habing, H.B. Dejonghe  
(Dordrecht: Kluwer), p. 209
- Kormendy, J. & McClure, R. D., 1993, AJ, 105, 1793

- Krist, J.E., 1997, in ‘The 1997 HST Calibration Workshop with a New Generation of Instruments’,  
p. 271
- Kuijken, K., & Merrifield, M., 1995, ApJ, 443, L13
- Lauberts A., Valentijn E.A., 1989, The Surface Photometry Catalog of the ESO-Uppsala Galaxies,  
ESO
- Lauer T., et al., 1995, AJ, 110, 2622
- Lauer, T. R., Faber, S. M., Ajhar, E. A., Grillmair, C. J., & Scowen, P. A., 1998, AJ, 116, 2263
- Matthews, L. D., & Gallagher, J. S., III, 1997, AJ, 114, 1899
- Matthews, L.D., et al. 1999, AJ, 118, 208
- Minniti, D., Olszewski, E. W., Riecke, M., 1993, ApJ, 410, L79
- Nilson, P., 1973, Uppsala General Catalog of Galaxies, Uppsala Astron. Obs. Ann., 6
- Norman C. A., Sellwood J. A., Hasan H., 1996, ApJ, 462, 114
- Oke J. B., & Gunn J. E., 1983, ApJ, 266, 713
- Peletier, R.F., Balcells, M., Davies, R.L., Andredakis, Y., Vazdekis, A., Burkert, A., Prada, F.,  
1999, MNRAS, 310, 703
- Pfenniger, D., Norman, C., 1990, ApJ, 363, 391
- Pfenniger, 1993, IAU Symposium 153, eds. Habing & Dejonghe, Dordrecht: Kluwer, p. 387
- Phillips, A. C., Illingworth, G. D., MacKenty, J. W., Franx, M., 1996, AJ, 111, 1566
- Seigar, M., Carollo, C.M., Stiavelli, M., de Zeeuw, P.T., Dejonghe, H., 2000, AJ, submitted (paper  
II)
- Shlosman, I., 1994, in ‘Mass-transfer induced activity in galaxies’, Cambridge University Press, p.  
406
- Shlosman, I., & Robinson, A., 1995, Observatory V.115, No. 1126/Jun, p. 154
- Shlosman, I., Begelman, M.C., & Frank, J., 1990, Nature, 345, 679

Wyse, R.F.G., Gilmore, G., Franx, M., 1997, ARAA, 35, 637

Fig. 1.— Panel a:  $H$  images (left) and  $V - H$  color maps (right) for 38 (out of 39, see text) galaxies observed with NICMOS which host a distinct nucleus and for which also WFPC2 images are available from our previous F606W survey. Panel b:  $H$  images (left) and  $J - H$  color maps (right) for the 5 galaxies observed in F160W which host a distinct nucleus and for which the only additional image available from our program is in the F110W filter. All images have North up and East left, and are  $9'' \times 9''$  size.

Fig. 2.— Same as Figure 1, but for the 25 galaxies which either do not host a distinct nucleus or in which the presence of a distinct nucleus is uncertain (19 objects with  $V - H$  color maps, panel a, and 6 objects with  $J - H$  color maps, panel b).

Fig. 3.— Panel a (left):  $H$  light profile of NGC 2082. The galaxy hosts a distinct nucleus, clearly visible on top of the underlying exponential bulge. Panel b (right):  $H$  light profile of NGC 2460. The galaxy hosts an  $R^{1/4}$ -law bulge and no detectable distinct nucleus.

Fig. 4.— A comparison of the sizes of the nuclei as determined from the F160W images and the F606W (triangles) or F110W (squares) images.

Fig. 5.— Panel a (left): The absolute magnitude versus half-light radius relation for the nuclei in the F160W passband. Panel b (right): For comparison, the same relation is plotted for the WFPC2 F606W passband. Triangles represent nuclei embedded in early- to intermediate-type hosts, S0a to Sc; filled squares are the four nuclei embedded in the Scd and later-type disks.

Fig. 6.— The  $V - H$  color of the nuclei versus the RC3 Hubble type of the host galaxy. Different symbols identify the four ‘classes’ of galaxies described in §3. In particular, filled triangles are the galaxies with concentrated nuclear star formation mixed with dust (class 1), open squares are the galaxies with diffuse blue nuclear regions (class 2), pentagons are the galaxies with regular nuclear/circum-nuclear dust (class 3), and 5-points stars are the galaxies with irregular nuclear/circum-nuclear dust (class 4).

Fig. 7.— The  $V - H$  color distribution for the nuclei (solid line) and the underlying host galaxy (dotted line). The latter colors are obtained integrating within  $3''$  the Nuker fits to the radial light profiles (profiles and fits presented in paper II).

Fig. 8.— Panel a: Absolute  $V$  magnitude versus  $V - H$  color for the nuclei. Panel b:  $J - H$  versus  $V - H$  color for the nuclei. Symbols are as in Figure 6.

Fig. 9.— The  $H$  images for the nine galaxies observed only in this filter.

Fig. 10.— Results of the tests performed for the subset of ‘really-observed’ galaxy-nucleus pairs to assess the accuracy of the recovered nucleus-parameters. Panel a: The distribution of the ratio between the recovered radius and the input radius of the simulated nucleus. Panel b: The distribution of the ratio between recovered- and input-flux of the nucleus. In Panels a and b the dashed line refers to modified-Hubble nuclei, the dotted line to Plummer nuclei, and the solid line to the sum of the two families. Panel c: The difference between input and recovered radius as a function of the difference between input and recovered luminosity of the nucleus, respectively. Empty symbols refer to modified-Hubble nuclei, filled symbols to Plummer nuclei.

Fig. 11.— Results of the general tests performed on a grid of power-law and exponential galaxies to assess the accuracy of the recovered parameters for the nuclei. Panel a: The difference between the recovered and input  $H_{AB}$  magnitude of the nucleus ( $\Delta mag$ ) versus the nuclear cusp slope  $\gamma$  for the power-law galaxies (left) and versus the exponential scale-length for the exponential galaxies (right). For both the power-law and the exponential galaxies, squares and triangles identify the brightest and the faintest sets of simulated host galaxies, respectively; the size of the symbols increases with increasing input scale length of the Plummer nucleus (1, 1.5, 2, 3, 4 and 5 pixels, respectively). Panel b: The recovered- versus the input-FWHM of the central nucleus for the power-law (left) and the exponential galaxies (right). Squares and triangles identify again the brightest and the faintest sets of simulated host galaxies. For the power-law galaxies, the size of the symbols increases for increasing  $\gamma$  (from 0 to 0.7 for the bright hosts, and from 0.5 to 0.7 for the faint hosts). For the exponential galaxies, the size of the symbols increases with increasing scale-length  $h$  of the exponential-type host ( $h = 5, 10, 25$  pixels). For reference, the solid line represents the effect of the PSF on an ‘isolated’ nucleus (in the absence of underlying galaxy). Panel c: The  $\Delta mag$  versus the input radius of the nucleus for the Nuker-law (left) and the exponential galaxies (right). For the power-law galaxies, symbols are crosses, empty triangles, empty squares and empty pentagons for the  $\gamma = 0.1, 0.3, 0.5, 0.7$  bright hosts, respectively; filled squares and pentagons represent instead the  $\gamma = 0.5, 0.7$  faint hosts. The size of the symbol increases with increasing input scale length of the Plummer nucleus (again 1, 1.5, 2, 3, 4 and 5 pixels, respectively). For the exponential galaxies, empty and filled symbols represent the bright and faint families of hosts, respectively; triangles, squares and pentagons represent respectively the  $h = 5, 10, 25$  cases; the size of the symbols increases with increasing input scale length of the nucleus. The solid line represents the effect of the PSF on an isolated nucleus.

Fig. 12.— Panel a (left): The difference between the recovered and the input magnitudes of a nucleus as a function of the input magnitude of the nucleus for the power-law galaxy models. Panel b (right): The similar plot for the exponential galaxy-models. The plots show that there is no systematic trend with luminosity, although the systematic errors increase with decreasing luminosity.

Fig. 13.— Results of the tests performed for the subset of ‘really-observed’ galaxy-nucleus pairs of Figure 9 to assess the error on the V-H colors. The histograms refer to nuclei modelled with either a modified Hubble profile (solid line), or a Plummer law (dotted line). The sum of the two histograms is a conservative benchmark for determining the error, given that the intrinsic shape of the nuclei is unknown. The partial cancellation of systematic effects, which are similar in both bands, leads to an error on the  $V - H$  color of  $\sim 0.4$  magnitudes.

This figure "carollo\_pap1\_final\_fig1a\_1.jpg" is available in "jpg" format from:

<http://arxiv.org/ps/astro-ph/0110281v1>



This figure "carollo\_pap1\_final\_fig1b\_1.jpg" is available in "jpg" format from:

<http://arxiv.org/ps/astro-ph/0110281v1>

This figure "carollo\_pap1\_final\_fig2a\_1.jpg" is available in "jpg" format from:

<http://arxiv.org/ps/astro-ph/0110281v1>

This figure "carollo\_pap1\_final\_fig2b\_1.jpg" is available in "jpg" format from:

<http://arxiv.org/ps/astro-ph/0110281v1>

Name	Filter	$D$ (Mpc)	Type	$m_B$ (mag)	$A_B$ (mag)	Bulge	Spectrum
E205G7	F606W, F110W	31	.SBR3..	15.02*	0.24	-	HII
E240G12	F606W, F110W	28	.S7....	14.35*	0.0	EXPO	HII
E404G3	F606W*, F110W	37	.SBT4..	14.04*	0.0	-	-
E498G5	F606W	37	.SXS4P.	13.54	0.42	EXPO	HII
E499G37	F606W	14	.XS7..	13.15*	0.17	EXPO	-
E548G29	F606W	24	.SB7...	14.19*	0.04	EXPO	-
E549G18	F606W, F110W	24	.SXT5..	13.49*	0.11	EXPO	-
E572G22	F606W, F110W	22	RSB.7P?	14.92*	0.08	EXPO	-
IC4390	F606W	30	.SXS4..	13.41*	0.40	-	HII
IC5271	F110W	27	.S..37.	12.34	0.04	-	-
IC5273	F606W*, F110W	21	.SBT6..	11.80	0.04	-	-
N289	F606W*, F110W	20	.SBT4..	11.70	0.02	-	-
N406	F606W, F110W	23	.SAS5..	13.04	0.05	EXPO	-
N488	F606W	37	.SAR3..	11.06	0.09	$R^{1/4}$	INT
N772	F110W	38	.SAS3..	10.92	0.17	-	INT
N972	F606W*, F110W	24	.S..2..	11.90	0.37	-	HII
N986	F606W	31	.SBT2..	11.61	0.03	-	HII
N1345	F606W	24	.SBS5P.	14.23	0.10	EXPO	-
N1398	F110W	20	PSBR2..	10.57	0.0	-	-
N1483	F606W	16	.SBS4..	13.11	0.0	EXPO	-
N1688	F606W	17	.SBT7..	12.00	0.0	-	-
N1800	F110W	12	.IBS9..	13.13	0.0	-	-
N1892	F606W	17	.S..6..	12.70	0.13	-	-
N2082	F606W, F110W	19	.SBR3..	12.47	0.15	EXPO	-
N2196	F606W, F110W	35	PSAS1..	11.37	0.45	$R^{1/4}$	-
N2339	F606W, F110W	36	.SXT4..	11.90	0.61	-	INT
N2344	F606W	14	.SAT5..	12.39	0.42	$R^{1/4}$	-
N2460	F606W	26	.SAS1..	12.58	0.14	$R^{1/4}$	-
N2566	F110W	25	PSBT2P.	10.35	1.48	-	-
N2748	F606W	24	.SA.4..	12.40	0.01	-	HII
N2758	F606W	30	PSB.4P?	13.46*	0.53	EXPO	-
N2964	F606W	20	.SXR4..	11.97	0.02	-	HII
N3067	F606W, F110W	23	.SAS2..	12.71	0.07	-	HII
N3259	F606W	27	.SXT4..	12.89	0.0	EXPO	-
N3277	F606W, F110W	21	.SAR2..	12.47	0.03	-	HII
N3455	F606W, F110W	19	PSXT3..	12.83*	0.02	EXPO	-
N3898	F606W	22	.SAS2..	11.60	0.0	$R^{1/4}$	INT
N3900	F606W	27	.LAR+..	12.13	0.07	$R^{1/4}$	AGN
N3928	F606W	17	.E?....	13.18	0.04	-	HII
N3949	F110W	12	.SAS4..	11.51	0.03	-	HII
N4102	F606W	13	.SXS3..	11.98	0.01	-	AGN
N4219	F606W	29	.SAS4..	12.10	0.61	-	-
N4384	F606W	37	.S..1..	13.50	0.0	-	HII
N4527	F110W	34	.SXS4..	11.36	0.02	-	INT
N4750	F606W, F110W	27	RSAT2..	12.04	0.03	-	AGN
N4806	F606W, F110W	37	.SBS5?.	13.09*	0.35	-	-
N4980	F606W	22	.SXT1P?	13.19*	0.34	EXPO	-
N5188	F606W, F110W	36	PSXS3P.	12.79	0.17	-	HII
N5377	F606W, F110W	22	RSBS1..	12.24	0.0	-	AGN
N5448	F606W	32	RSXR1..	11.89	0.04	-	AGN
N5678	F606W*, F110W	30	.SXT3..	12.11	0.02	-	INT
N5806	F606W, F110W	29	.SXS3..	12.23	0.17	-	INT
N5985	F606W, F110W	46	.SXR3..	11.85	0.02	$R^{1/4}$	AGN
N6000	F606W	32	.SBS4..	12.30*	0.72	-	-
N6239	F606W, F110W	14	.SBS3P.	12.93	0.01	-	HII
N6340	F606W	18	.SAS0..	11.66	0.21	$R^{1/4}$	AGN
N6384	F606W, F110W	26	.SXR4..	10.70	0.44	EXPO	INT
N6810	F606W, F110W	30	.SAS2..	12.19	0.18	-	INT
N6951	F110W	22	.SXT4..	11.68	0.94	-	AGN
N7013	F606W	13	.SAR0..	11.10	1.30	-	AGN
N7162	F606W*, F110W	33	.SAS5..	13.29	0.0	-	-
N7177	F110W	18	.SXR3..	12.01	0.25	-	INT
N7188	F606W*, F110W	27	PSBT4..	13.95*	0.07	-	-
N7217	F110W	15	RSAR2..	11.02	0.44	-	AGN
N7259	F606W*, F110W	26	.S..3..	13.88*	0.0	-	-
N7280	F606W	28	.LXR+..	12.78	0.23	$R^{1/4}$	AGN
N7421	F606W, F110W	26	.SBT4..	12.48	0.04	-	Q
N7513	F110W	24	PSBS3P.	11.96	0.19	-	-
N7690	F606W, F110W	21	.SAR3..	13.00	0.0	-	HII

Table 1: The 69 galaxies of our sample observed with NICMOS Camera-2 in F160W. The column ‘Filter’ lists the additional passbands in which these galaxies have also been observed in our program (an asterisk close to the F606W filter identifies the 8 galaxies for which the analysis of the WFPC2 photometry is not included in our previous papers, due to their delayed observations). The remaining columns give the distance in Mpc, the morphological type and the apparent total B magnitude from the RC3 (asterisks indicate Cousins B measurements), and the  $B$  extinction from Burstein & Heiles (1984). The column ‘Bulge’ reports whether the galaxies host either an  $R^{1/4}$  or an exponential bulge, based on the analysis of our WFPC2 images (the radial extent of the NICMOS data is insufficient to properly perform a bulge/disk decomposition). When available, in the last column we report the information on the central spectral properties shown by the system at ground-based resolution (HII = HII-type; AGN = AGN-type, INT = Intermediate between HII and AGN; Q = Quiescent; information extracted from Ho et al. 1997, and from our own unpublished spectra, Carollo, Chiappini & Heckman 2001, in preparation).

Name	$m_V$ (mag)	$R_V$ ( $''$ )	$m_J$ (mag)	$R_J$ ( $''$ )	$m_H$ (mag)	$R_H$ ( $''$ )
E205G7	19.2(0.2)	0.05(0.02)	17.7(0.6)	0.12(0.02)	17.3(0.8)	0.12(0.02)
E240G12	22.2(0.1)	0.02(0.02)††	21.4(0.5)	0.02(0.02)	21.2(0.6)	0.03(0.02)
E404G3*	22.1(0.4)	0.054(0.08)	20.9(0.3)	0.08(0.01)	20.8(0.9)	0.03(0.02)
E498G5	20.0(0.1)	0.04(0.02)	-	-	18.7(0.3)	0.05(0.02)
E499G37	20.6(0.7)	0.36(0.05)	-	-	20.3(0.2)	0.28(0.06)
E548G29	21.8(0.4)	0.08(0.03)	-	-	20.6(0.6)	0.04(0.01)
E549G18	23.3(0.1)	0.09(0.01)	20.7(0.3)	0.10(0.01)	20.3(0.7)	0.17(0.07)
E572G22	21.8(0.1)	0.06(0.02)	21.2(0.2)	0.04(0.01)	21.1(0.4)	0.04(0.01)
IC4390	18.1(0.3)	0.26(0.09)	-	-	16.4(0.3)	0.17(0.08)
IC5271	-	-	16.8(0.1)	0.13(0.02)	16.4(0.2)	0.11(0.03)
IC5273*	no nucleus	-	-	-	-	-
N289*	19.8(0.6)	0.14(0.03)	17.3(0.2)	0.14(0.06)	16.7(0.2)	0.13(0.03)
N406	21.6(0.3)	0.04(0.01)	21.0(0.3)	0.07(0.02)	20.9(0.3)	0.10(0.08)
N488	no nucleus	-	-	-	-	-
N772	no nucleus	-	-	-	-	-
N972*	?	?	?	?	?	?
N986	16.0(0.4)	0.18(0.05)	-	-	16.5(0.5)	0.11(0.01)
N1345	21.1(0.3)	0.05(0.01)	-	-	20.4(0.1)	0.05(0.02)
N1398	no nucleus	-	-	-	-	-
N1483	21.8(0.2)	0.02(0.02)††	-	-	21.6(0.5)	0.03(0.02)
N1688	19.6(0.3)	0.11(0.05)	-	-	19.2(0.8)	0.06(0.04)
	19.8(0.3)	0.12(0.05)	-	-	19.8(0.7)	0.03(0.03)
N1800	no nucleus	-	-	-	-	-
N1892	21.2(0.7)	0.07(0.01)	-	-	18.5(0.3)	0.05(0.01)
N2082	21.0(0.3)	0.08(0.01)	19.8(0.5)	0.08(0.01)	19.4(0.7)	0.06(0.01)
N2196	no nucleus	-	-	-	-	-
N2339	?	?	?	?	?	?
N2344	no nucleus	-	-	-	-	-
N2460	no nucleus	-	-	-	-	-
N2566	-	-	14.6(0.5)	0.12(0.03)	14.3(0.7)	0.11(0.01)
N2748	?	?	?	?	?	?
N2758	20.4(0.3)	0.11(0.05)	-	-	20.2(0.6)	0.07(0.01)
N2964	18.4(0.5)	0.12(0.04)	-	-	16.2(0.4)	0.14(0.04)
N3067	?	?	?	?	?	?
N3259	19.5(0.1)	0.02(0.02)††	-	-	18.4(0.7)	0.11(0.08)
N3277	17.3(0.3)	0.17(0.01)	16.0(0.2)	0.14(0.02)	15.7(0.2)	0.15(0.02)
N3455	20.2(0.2)	0.07(0.01)	19.2(0.3)	0.10(0.01)	18.9(0.4)	0.04(0.01)
N3898	no nucleus	-	-	-	-	-
N3900	no nucleus	-	-	-	-	-
N3928	17.1(0.3)	0.10(0.05)	-	-	16.6(0.2)	0.10(0.01)
N3949	-	-	18.0(0.3)	0.04(0.03)	17.8(0.5)	0.05(0.03)
N4102	?	?	?	?	?	?
N4219	?	?	?	?	?	?
N4384	21.78(0.3)	0.08(0.03)	-	-	21.5(0.8)	0.06(0.04)
N4527	-	-	?	?	?	?
N4750	18.0(1.0)†	0.11(0.05)†	16.8(0.2)	0.15(0.03)	16.3(0.3)	0.14(0.03)
N4806	20.9(0.2)	0.07(0.01)	19.9(0.4)	0.11(0.02)	19.4(0.5)	0.05(0.01)
N4980	20.3(0.2)	0.07(0.02)	20.0(0.2)	0.07(0.01)	19.7(0.3)	0.05(0.01)
N5188	19.3(0.3)	0.08(0.01)	17.2(0.3)	0.24(0.12)	16.6(0.1)	0.20(0.09)
N5377	16.3(0.2)	0.26(0.01)	15.7(0.7)	0.19(0.02)	15.8(0.2)	0.18(0.03)
N5448	?	?	-	-	?	?
N5678*	?	?	16.8(0.2)	0.21(0.03)	16.4(0.3)	0.18(0.06)
N5806	18.7(0.5)	0.15(0.02)	16.7(0.3)	0.22(0.06)	16.3(0.3)	0.21(0.06)
N5985	?	?	?	?	?	?
N6000	17.6(0.4)	0.21(0.07)	-	-	16.6(0.4)	0.17(0.05)
N6239	20.96(0.5)†	0.03(0.02)†	19.4(0.5)	0.05(0.02)	18.6(0.6)	0.03(0.03)
N6340	no nucleus	-	-	-	-	-
N6384	19.7(0.6)	0.10(0.02)	17.9(0.7)	0.12(0.04)	17.6(0.8)	0.14(0.05)
N6810	saturated	-	?	?	?	?
N6951	-	-	16.4(0.2)	0.17(0.04)	16.0(0.3)	0.18(0.06)
N7013	no nucleus	-	-	-	-	-
N7162*	21.0(0.1)	0.11(0.04)	19.9(0.4)	0.11(0.02)	19.8(0.6)	0.11(0.03)
N7177	-	-	?	?	?	?
N7188*	19.9(0.4)	0.10(0.04)	19.3(0.3)	0.12(0.01)	18.9(0.3)	0.06(0.02)
N7217	no nucleus	-	-	-	-	-
N7259*	20.6(0.6)	0.09(0.02)	19.3(0.3)	0.07(0.01)	18.8(0.3)	0.06(0.03)
N7280	no nucleus	-	-	-	-	-
N7421	19.1(0.5)	0.07(0.03)	17.9(0.5)	0.09(0.01)	17.6(0.8)	0.11(0.02)
N7513	-	-	18.6(0.3)	0.12(0.02)	18.3(0.4)	0.06(0.01)
N7690	18.1(0.7)	0.09(0.01)	16.8(0.3)	0.13(0.08)	16.7(0.3)	0.17(0.05)

Table 2: Apparent magnitudes ( $m_{band}$ ) and half-light radii ( $R_{band}$ ) for the nuclei in the  $V$ ,  $J$  and  $H$  bands. The optical measurements are included for easy reference; they are extracted from Carollo et al. (1997, 1998) for all galaxies but for the eight identified by an asterisk (see caption Table 1, and text). Galaxies observed with NICMOS that do not host a photometrically-distinct nucleus are also listed for completeness (and identified by ‘no nucleus’ in the second column). Question marks (?) identify systems in which the presence of a nucleus is unclear. A dagger (†) in column 3 identifies the two nuclei for which  $V$  measurements of their sizes and magnitudes were possible only after analysing the NIR images, which revealed the location of the true center/nucleus. A double-dagger (††) identifies nuclei that are unresolved on the PC of WFPC2.

Name	Centered?	Elongated?	Color?	Bar?	Comments
E205G7	Y	N	B	L	red (dust) ring at $\sim 1''$ radius; red (dust) lane down to nucleus
E240G12	?	?	N	?	round nucleus embedded in fainter elongated structure;
E404G3	?	N	B	N?, L	several blue features (major one is shock-front-like, East of nucleus)
E498G5	Y	N	?	N?	inner elongated structure is warped
E499G37	Y	N	B	S	blue star forming spiral arms and red (dust) spiral-like lanes
E548G29	?	N	?	L	over smooth round bulge
E572G22	?	N	N	L?	Faint star forming spiral arm reaches smooth round 'bulge' at $\sim 1''$
IC4390	Y	N	N?	S?, L	red (dust) patches and blue features down to nucleus
IC5271	Y	?	B?	S?, L	NE feature with blue and red knots
IC5273	-	-	-	S?, L	red (dust) lane across nucleus; nuclear bar or disk
NGC289	?	?	?	S?, L?	red bar/lane feature NE of nucleus
NGC406	N	N	B?	N	multiple-knots, elongated central blue feature (not considered as 'nucleus');
NGC488	-	-	-	N	red (dust) patch NE of center
NGC772	-	-	-	N	red (dust) lane across (NW of red) center
NGC972	?	?	?	?	red (dust) and blue star forming knots down to nucleus;
NGC986	?	?	B	L	triple blue structure $\approx 10''$ NW of nucleus (background?)
NGC1345	?	?	N	L	red (dust?) spot at center;
NGC1398	-	-	-	N	red (dust) spiral lanes down to center
NGC1483	?	?	B	?	red (dust) spiral lane down to blue center
NGC1688	?	?	?	L	central region obscured by dust
NGC1800	?	?	?	L?	blue knots (on bar and spiral arms) and red (dust) lanes down to nucleus
NGC1892	?	?	R	N	red (dust) patches down to nucleus; star forming knots
NGC2082	?	N	R	L	center is blue; blue feature $\approx 4''$ SE of center
NGC2196	-	-	-	N	several cluster-like blue star forming knots in the nuclear region
NGC2339	?	?	?	S?	center not well defined even in $H$
NGC2344	-	-	-	N	large number of cluster/star-type blue sources
NGC2460	-	-	-	N	red (dust) lane across nucleus (reddened)
NGC2566	Y	N	?	N	red (dust) and blue (star forming) regions throughout central region
NGC2748	?	?	?	N	spiral red (dust) feature SE of center (down to reddened center)
NGC2758	N	N	N	N	red center is clearly dust-reddened; blue source SW of center;
NGC2964	Y	Y	N	N	blue-NE/red-SW oriented bar-like feature
NGC3067	?	?	?	N	no major features in color map ( $\sim 0.2$ mag central reddening)
NGC3259	Y	N	B	N	blue center; blue features on spiral pattern down to center;
NGC3277	Y	N	R	N	red (dust) spiral features down to center
NGC3455	?	N	N	S?	regular blue nuclear spiral arms; red (dust) lanes outside
NGC3898	-	-	-	S?, L?	dust throughout central region
NGC3900	-	-	-	N	faint red (dust) lanes through center
NGC3928	Y	N	B	N	spiral structure and red (dust) features down to center; reddened nucleus?
NGC3949	Y	N	B	S?	center has same color than surroundings; dust throughout central region
NGC4102	?	?	?	S?, L	floculent nuclear blue spiral arms and red (dust) lanes
NGC4219	?	?	?	S?	red (dust) spiral features down to reddened nucleus
NGC4384	?	?	N	S	faint red (dust) patches in central region; nuclear spiral arms (and bar?)
NGC4527	?	?	?	L?	red (dusty) center; red nuclear elongated feature;
NGC4750	Y	N	?	S, L	larger scale SE-NW red (dust?) disk/barlike feature
NGC4806	Y	N	R	S?, L	connects with red spiral feature NE of center
NGC4980	N	N	R	N	center likely reddened by dust; red (dust) patches surround center
NGC5188	?	?	?	N	small scale regular spiral structure centered on nucleus;
NGC5377	Y	Y	B	L	red/ (dust) feature surrounds nucleus
NGC5448	Y	N	R?	S	nuclear barlike feature (?);
NGC5678	Y	?	B?	S?	red (dust) lane $\approx 0.7''$ N of nucleus
NGC5806	Y	?	?	S	center likely obscured by spiral dust feature;
NGC5985	-	-	-	L	nuclear star forming ring (or bar/arm)
NGC6000	?	?	B	L	irregular red (dust) patterns down to center (nucleus obscured/reddened?)
NGC6239	Y?	?	R	L?	dust (from disk) obscures center; likely no nucleus
NGC6340	-	-	-	N	red (dust) spiral features down to center (strongest NE of it)
NGC6384	Y	N	R	L?	red (dust) lane across nucleus (reddened)
NGC6810	?	Y	B	S?	granular appearance
NGC6951	Y	N	B?	N	dust in central region; location of center unclear;
NGC7013	-	-	-	N	nucleus parameters in Table 2 given for
NGC7162	Y	?	B?	S?	blue feature N of central red (dust) patch
NGC7177	?	?	?	S?, L	regular NE/SW-oriented red (dust) ring $\approx 5''$ from nucleus;
NGC7188	?	Y	N	N	inner ring-like red (dust) features
NGC7217	-	-	-	N	red nuclear bar along nucleus orientation
NGC7259	?	?	R	N	nucleus embedded in mini-bar? nuclear red (dust) ring around nucleus
NGC7280	-	-	-	S, L	clear bulge+bar structure in $H$ image (obscured by dust in $V$ )
NGC7421	Y	N	B?	L	red (dust) spiral structure across nucleus
NGC7513	Y	N	R	N	red (dust) lanes surround center
NGC7690	Y	?	?	S?	nucleus surrounded by irregular red (dust) ring;
					red (dust) spiral features down to ring
					irregular dust/star-formation
					red (dust) disk $\approx 0.6''$ diameter surrounds center;
					disklike red (dust) lane SW of center on slightly larger scales
					spiral/ringlike red (dust) feature down to dusty nucleus
					$V$ image is saturated; nucleus bluer than in $V - H$ color map;
					ubiquitous dust in central region
					blue ring surrounds red center; red (dust) spiral lanes outside blue ring
					ubiquitous dust from disk in central region (including center)
					NE-SW red bar (or ring/disk) feature; red (dust) lane E of nucleus
					red (dust) disk/spiral-like lanes across center; blue large-scale bar
					dust NW of nucleus
					blue disklike feature N of red center; blue 'arm' (strongest patch $\approx 5''$ from center)
					nucleus embedded in (elongated?) red feature; nuclear red (dust) lanes
					reddened center; red (dust) ringlike feature W of minor axis
					patchy red (dust) lanes down to nucleus
					irregular circumnuclear dust
					red (dust) disk surrounds blue disk/bar feature (central 'hole' in disk?)

**Table 3:** Notes on individual galaxies. The column ‘Centered?’ lists whether the photometrically-distinct nucleus – when present – is located (Y) or not (N) on the dynamical center of the host galaxy. The column ‘Elongated?’ lists whether the nucleus is round (N) or elongated (Y) in projection. The column ‘Color?’ identifies nuclei which are bluer (B) or redder (R) than their surroundings. An ‘N’ in this column indicates that the nucleus has a ‘normal’ color (i.e., similar to the circumnuclear region). The information is extracted from the  $V - H$  color maps or, for the galaxies observed only with NICMOS, from the  $J - H$  color maps. The column ‘Bar?’ lists whether a large- (L) or small- (S) scale bar is present in the system. Question marks indicate uncertain detections due to a very complex central structure.

Name	$D$ (Mpc)	Type	$m_B$ (mag)	$A_B$ (mag)	$m_H$ (mag)	$R_H$ ( $''$ )
NGC1365	26	.SBS3..	10.32	0.00	14.1(0.2)	0.04(0.01)
NGC2903	9	.SXT4..	9.61	0.07	17.8(0.4)	0.14(0.04)
NGC3031	?	.SAS2..	7.75	0.14	14.9(0.3)	0.05(0.02)
NGC4536	29	.SXT4..	11.16	0.00	?	?
NGC4565	18	.SAS3..	10.39	0.03	?	?
NGC4569	?	.SXT2..	10.17	0.09	15.2(0.5)	0.09(0.02)
NGC6217	21	RSBT4..	11.65	0.14	17.2(0.3)	0.12(0.04)
NGC7479	37	.SBS5..	11.44	0.16	-	-
NGC7742	26	.SAR3..	12.25	0.10	-	-

Table 4: The nine galaxies for which only F160W images are available. The columns give the distance in Mpc (derived from the RC3 recession velocity; for NGC3031 and NGC4569 the RC3 lists -34 and -331 km/s, respectively), the morphological type and the apparent total B magnitude from the RC3, and the  $B$  extinction from Burstein & Heiles (1984). The last two columns list the  $H$  magnitudes and the half-light radii for their nuclei (when present).

This figure "carollo\_pap1\_final\_fig1a\_2.jpg" is available in "jpg" format from:

<http://arxiv.org/ps/astro-ph/0110281v1>



This figure "carollo\_pap1\_final\_fig2a\_2.jpg" is available in "jpg" format from:

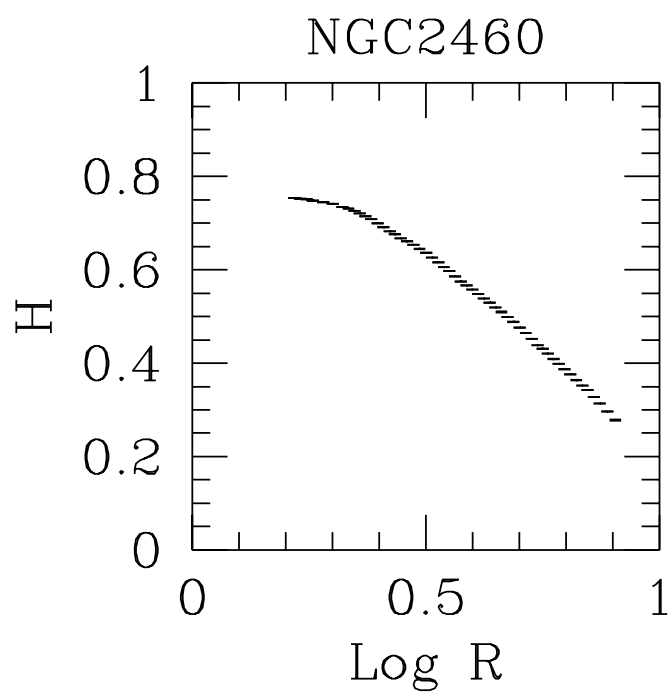
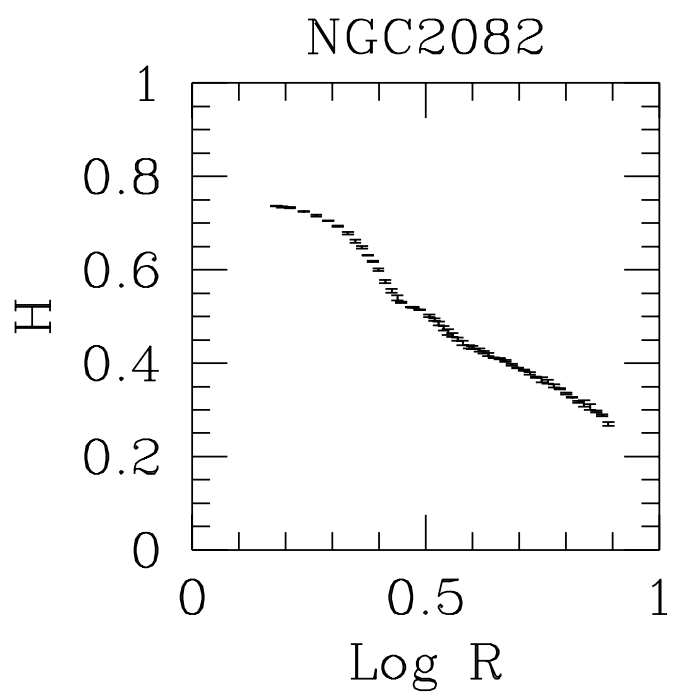
<http://arxiv.org/ps/astro-ph/0110281v1>

This figure "carollo\_pap1\_final\_fig1a\_3.jpg" is available in "jpg" format from:

<http://arxiv.org/ps/astro-ph/0110281v1>

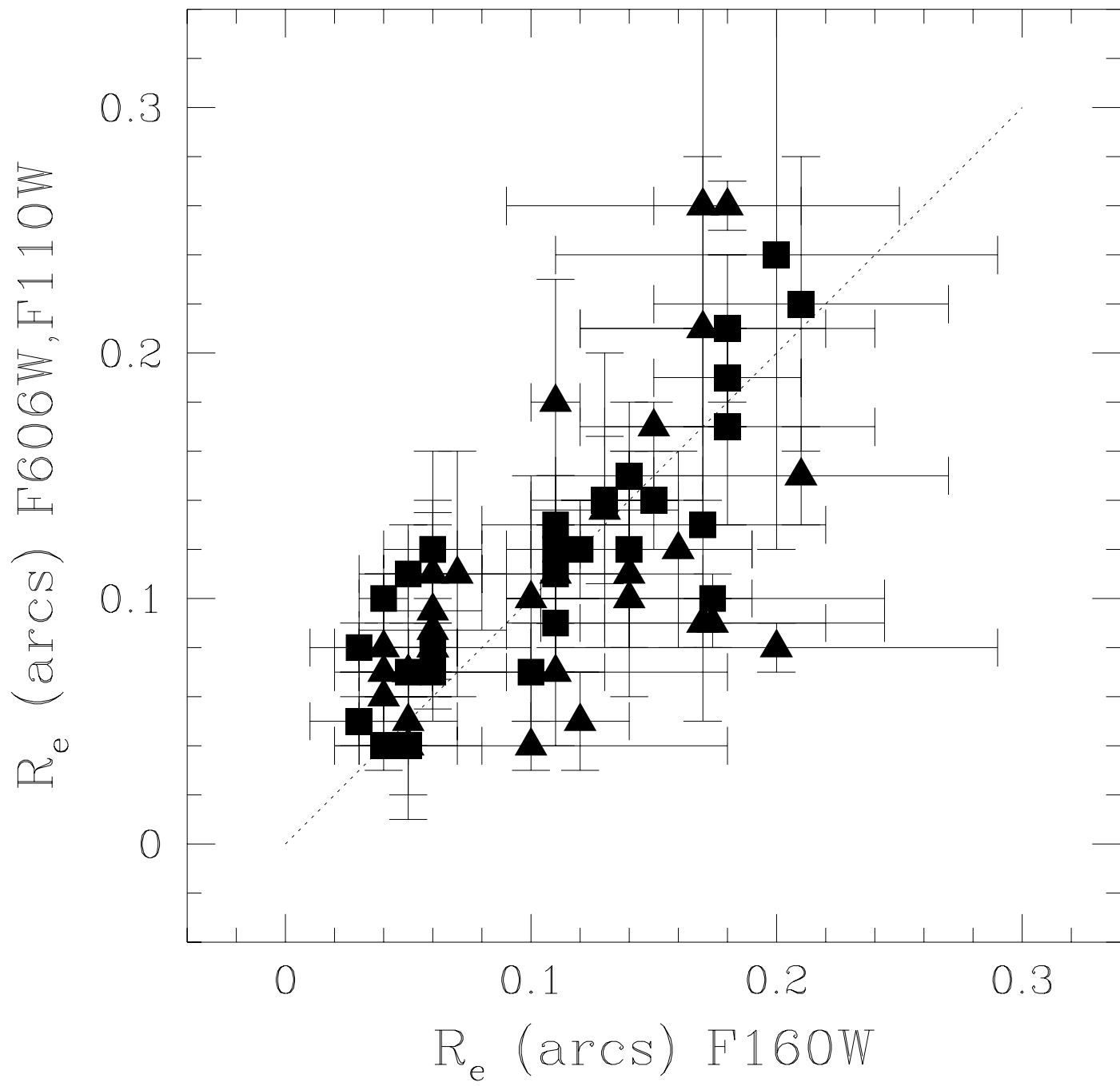
This figure "carollo\_pap1\_final\_fig2a\_3.jpg" is available in "jpg" format from:

<http://arxiv.org/ps/astro-ph/0110281v1>



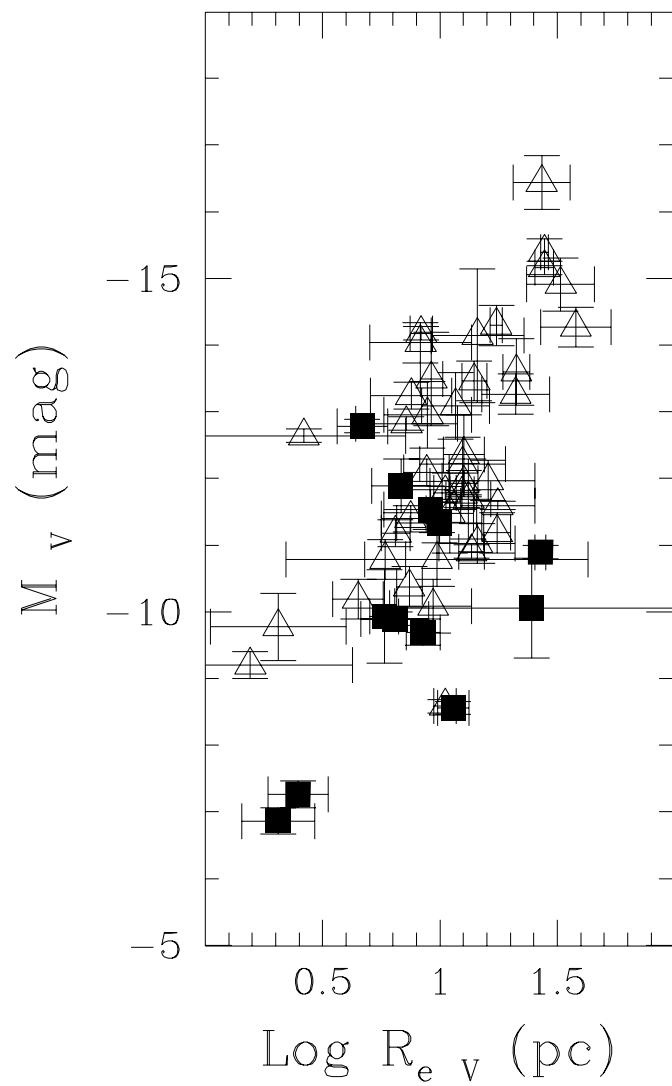
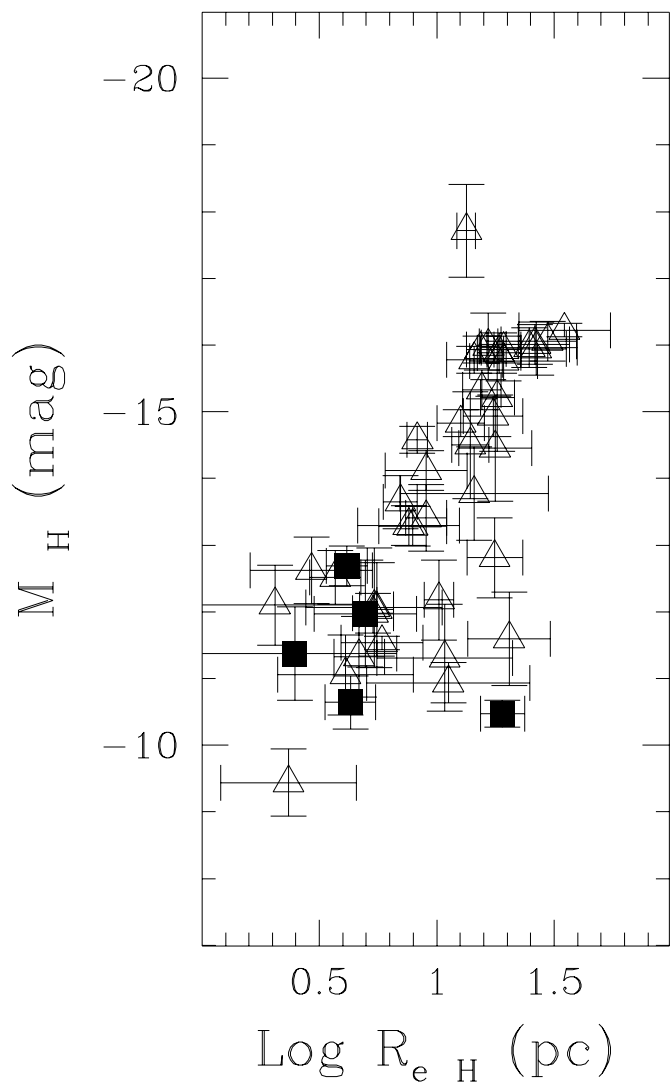
This figure "carollo\_pap1\_final\_fig1a\_4.jpg" is available in "jpg" format from:

<http://arxiv.org/ps/astro-ph/0110281v1>

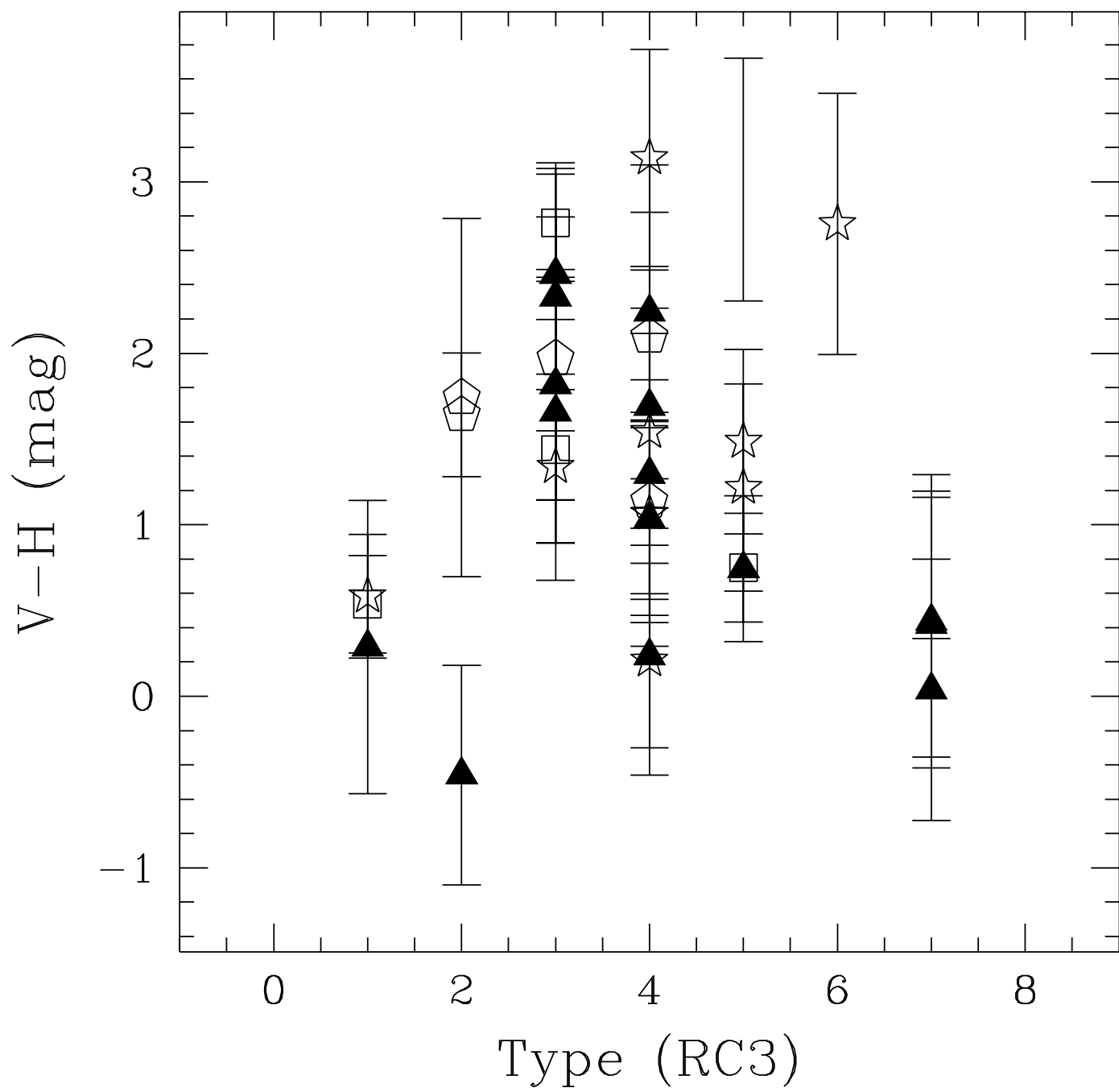


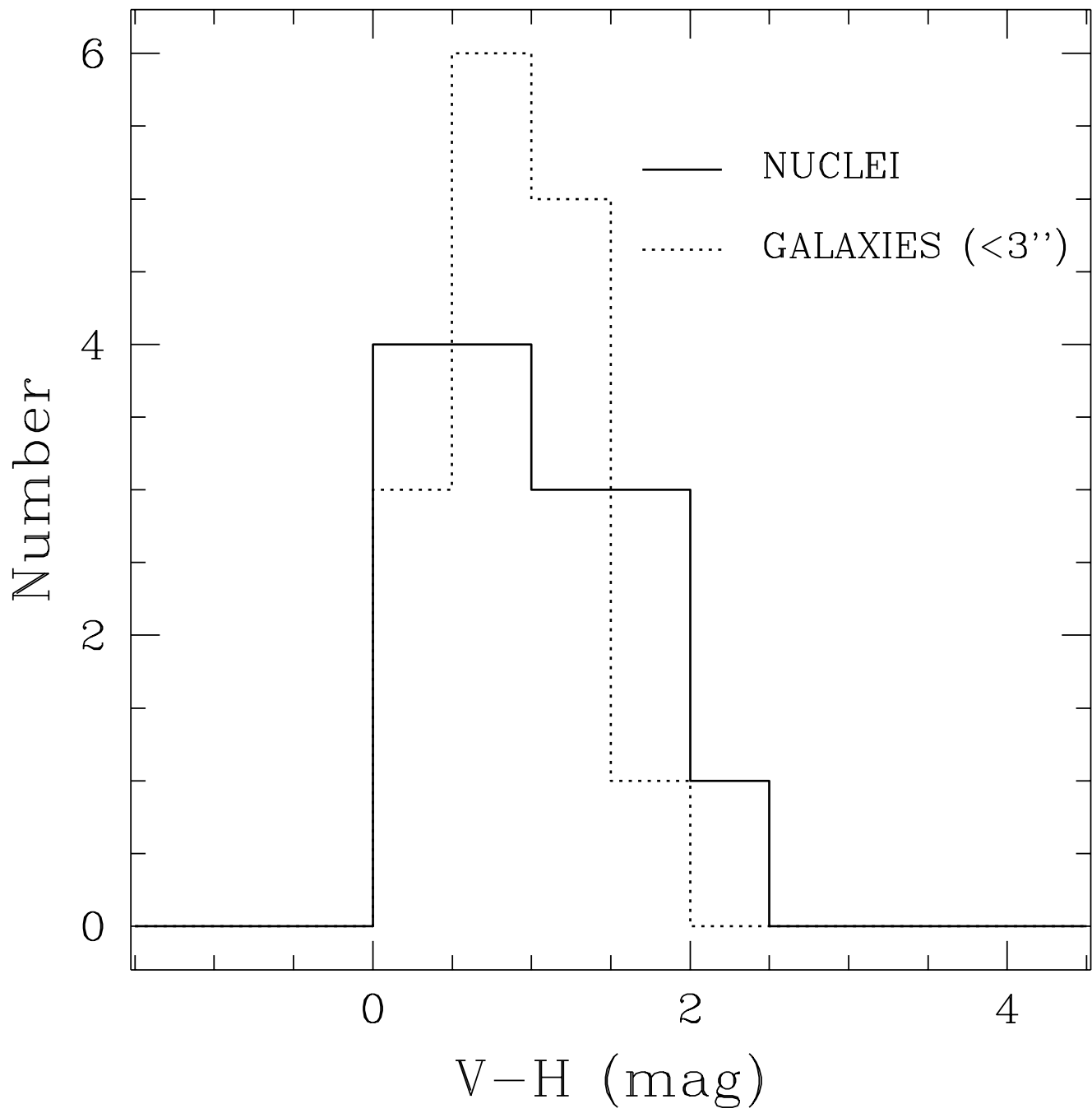
This figure "carollo\_pap1\_final\_fig1a\_5.jpg" is available in "jpg" format from:

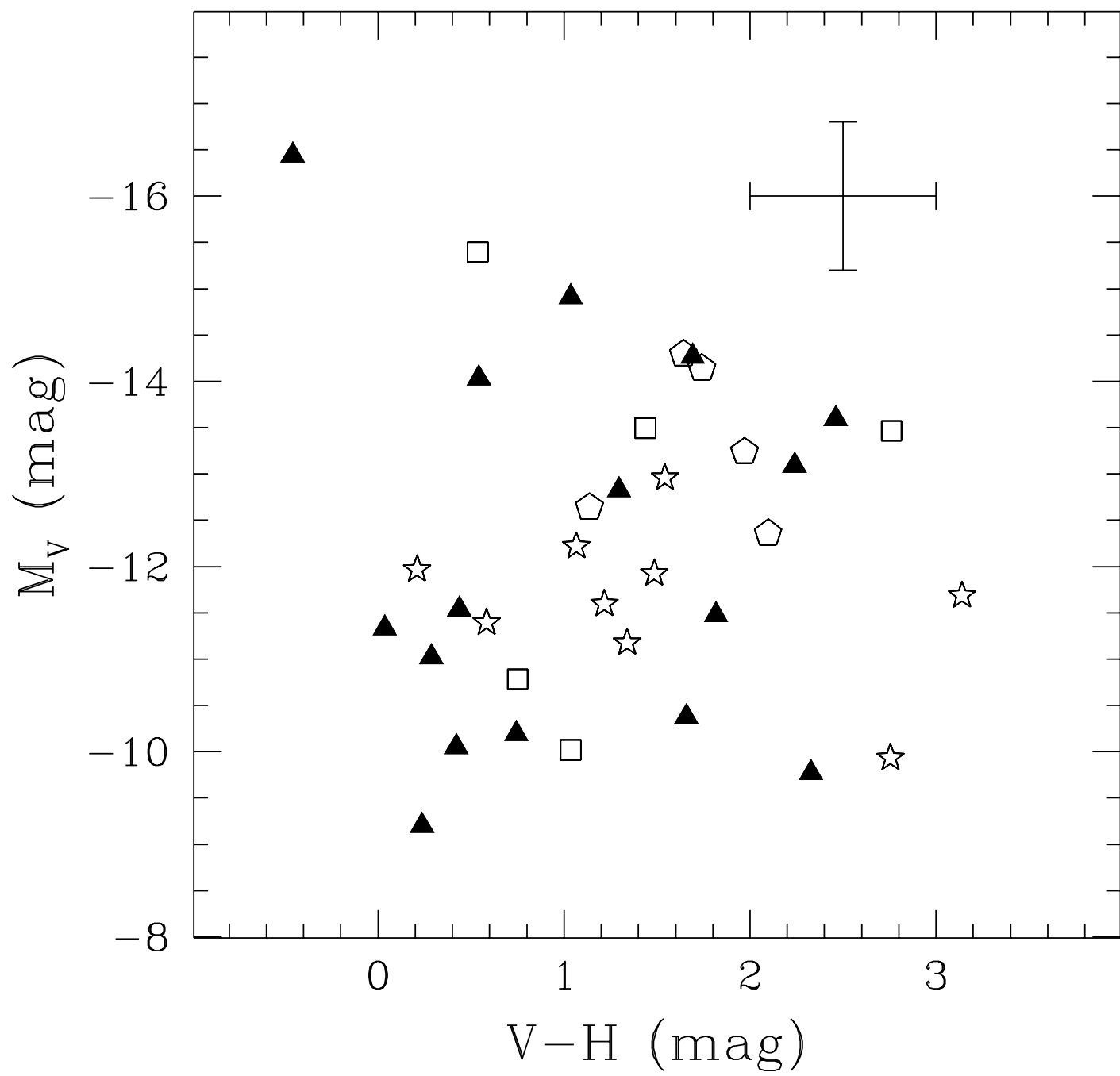
<http://arxiv.org/ps/astro-ph/0110281v1>

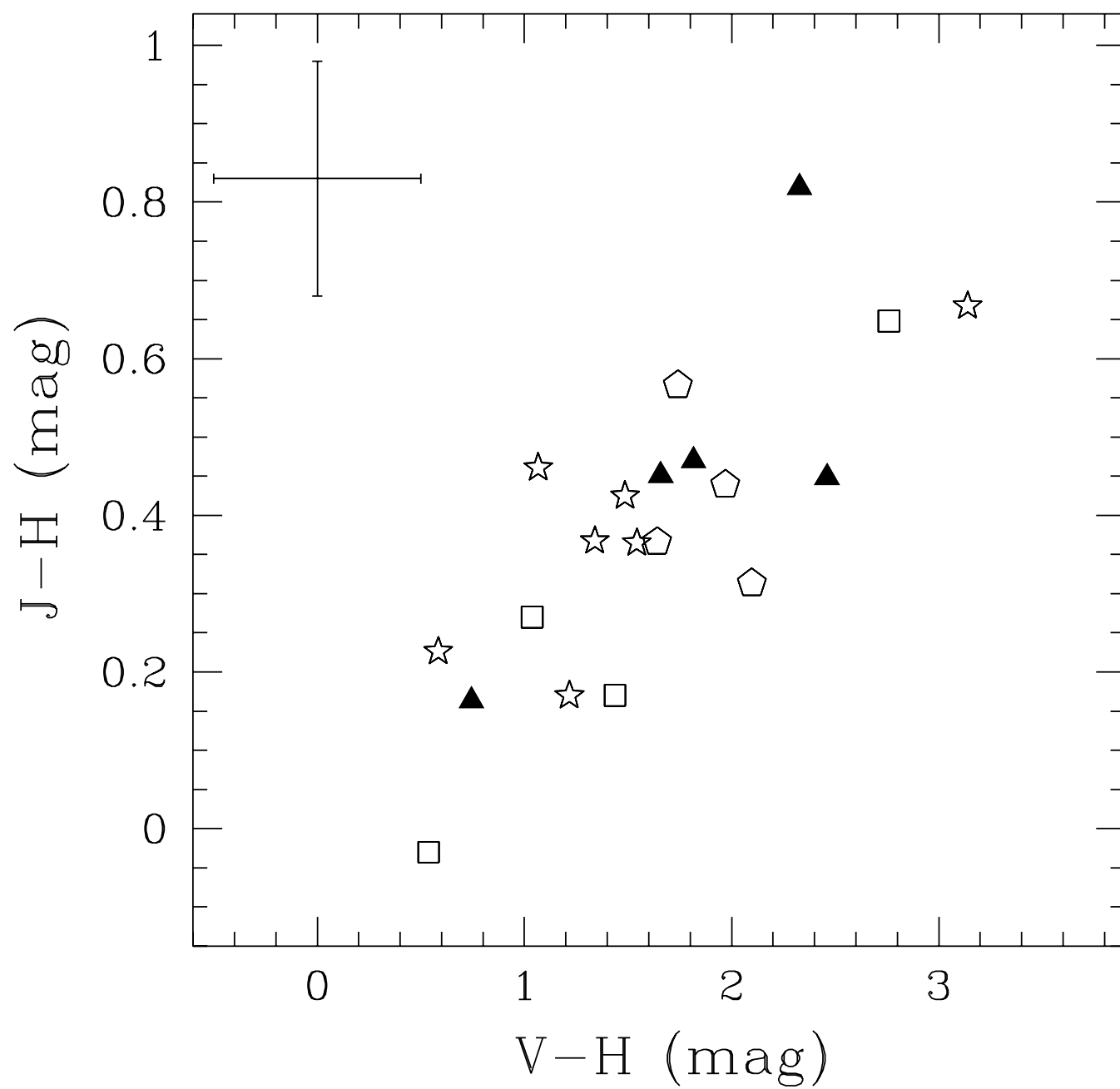












This figure "carollo\_pap1\_final\_fig9.jpg" is available in "jpg" format from:

<http://arxiv.org/ps/astro-ph/0110281v1>

